Mechanisms of decarboxylation of phenylacetic acids and their sodium salts in water at high temperature and pressure

Christopher R. Glein [a,b,*], Ian R. Gould [c], Edward D. Lorance [d],
Hilairy E. Hartnett [a,c], Everett L. Shock [a,c]

[a] *School of Earth and Space Exploration, Arizona State University, Tempe, AZ 85287-1404, USA*
[b] *Space Science and Engineering Division, Southwest Research Institute, San Antonio, TX 78228-0510, USA*
[c] *School of Molecular Sciences, Arizona State University, Tempe, AZ 85287-1604, USA*
[d] *Department of Chemistry, Vanguard University, Costa Mesa, CA 92626-9601, USA*

Abstract

Mechanistic interpretations of how organic reactions happen can enhance the predictive capacity of models for geochemical transformations built on thermodynamic and kinetic relations. In this study, the mechanisms of hydrothermal carboxylic acid decarboxylation reactions are explored using aqueous solutions of the model compound phenylacetic acid, its ring-substituted derivatives, and their sodium salts. Time-series experiments in gold capsules are performed at 300 °C and 1034 bar, and analyzed using gas chromatography. The decarboxylation products are the appropriately substituted toluene and CO_2 or HCO_3^- depending on the pH. It is found that the decarboxylation reaction is irreversible at the studied conditions, consistent with the expectation of a strong thermodynamic drive at elevated temperatures. Decarboxylation of both the acid and anion forms of phenylacetic acid follow first-order kinetics, with apparent rate constants of $0.044 \pm 0.005 \ h^{-1}$ ([1.2 $\pm 0.14] \times 10^{-5} \ s^{-1}$) and $0.145 \pm 0.02 \ h^{-1}$ ([4.0 $\pm 0.56] \times 10^{-5} \ s^{-1}$), respectively. However, trends in the reaction rate with changes in the electronic properties of methyl and fluoro substituents reveal that the two forms of phenylacetic acid decarboxylate via two different mechanisms. It is inferred that the associated phenylacetic acid molecule decarboxylates by the formation of a ring-protonated zwitterion, whereas the acid anion directly decarboxylates to a benzyl anion. Zwitterionic mechanisms of activation to decarboxylation may be applicable to other aromatic acids (*e.g.*, benzoic acid) having unsaturation that is *alpha*- or *beta*- to the carboxyl group, as well as to aliphatic acids that can be converted to α,β- or β,γ-unsaturated acids in natural hydrothermal systems. For acids lacking suitable unsaturation (*e.g.*, acetic acid) or at higher pH, carbanion mechanisms may predominate in hydrothermal fluids. In these cases, there is potential to predict decarboxylation rates from the pK_a of the hydrocarbon product. The finding of speciation-dependent reaction mechanisms implies that host rocks of aqueous fluids are key to determining decarboxylation rates, as a consequence of water-rock reactions that control fluid pH.
© 2019 Published by Elsevier Ltd.

Keywords: Hydrothermal organic transformations; Decarboxylation; Reaction mechanisms; Reaction rates

1. GEOCHEMICAL ORGANIC TRANSFORMATIONS

The fate of organic compounds at elevated temperatures and pressures governs organic-inorganic transitions in the deep carbon cycle on Earth (Manning et al., 2013; Shock et al., 2013; Sverjensky et al., 2014), the potential for abiotic

* Corresponding author at: Space Science and Engineering Division, Southwest Research Institute, San Antonio, TX 78228-0510, USA

E-mail address: christopher.glein@swri.org (C.R. Glein).

organic synthesis during fluid-rock reactions in icy ocean worlds (Postberg et al., 2018), and perhaps the geochemical processes from which biochemistry emerged (Shock and Boyd, 2015; Canovas and Shock, 2016; Martin, 2016; Weiss et al., 2016; Sousa et al., 2018). Processing of organic compounds at shallow and deep submarine hydrothermal systems has emerged as a focus of efforts to quantify fully the marine carbon cycle upon which life in the oceans and within the oceanic crust depends (Lang et al., 2010; 2012; 2013; 2018; Hawkes et al., 2015; 2016; Klein et al., 2015; McDermott et al., 2015; LaRowe et al., 2017; Fortunado et al., 2018; Tully et al., 2018). Meanwhile, the growing recognition that organic transformations can feed the deep biosphere in seafloor sediments (Wellsbury et al., 1997; Heuer et al., 2009; Riedinger et al., 2015; Walsh et al., 2016; Trembath-Reichert et al., 2017; Bradley et al., 2018; Graw et al., 2018; Kevorkian et al., 2018; Reese et al., 2018; Zinke et al., 2018), continental sedimentary basins (Fredrickson and Balkwill, 2006; Flores et al., 2008; Ulrich and Bower, 2008; Fry et al., 2009; Breuker et al., 2011; Schlegel et al., 2011; Wouters et al., 2013; Parnell and McMahon, 2016; Robbins et al., 2016), and throughout subsurface habitats in crystalline rocks (Pedersen and Ekendahl, 1990; Pedersen, 1997; Onstott et al., 2003; Lin et al., 2006; Sahl et al., 2008; Fukuda et al., 2010; Konno et al., 2013; Suzuki et al., 2014; Ino et al., 2016; 2018; Magnabosco et al., 2016; Simkus et al., 2016; Momper et al., 2017; Parnell et al., 2017; Drake et al., 2018; Walter et al., 2018), calls attention to how such reactions allow the expansion of life into the Earth's crust.

Predicting which organic transformations happen where and when is enabled by thermodynamic and kinetic models that attain maximum rigor when coupled with mechanistic understanding of how reactions occur. The focus of this investigation is to determine the mechanisms of decarboxylation of a suite of aromatic acids and acid anions. Decarboxylation is a major irreversible step in geochemical organic transformations that influences how petroleum hydrocarbons form in source rocks and are altered at reservoir conditions (Seewald, 2001a; 2001b; 2003), and can determine whether carboxylic acids are found in the geochemical and cosmochemical records (Cooper and Bray, 1963; Shimoyama and Johns, 1971; Willey et al., 1975; Carothers and Kharaka, 1978; Fisher, 1987; Means and Hubbard, 1987; Somerville et al., 1987; Shock, 1988; 1989; 1994; 1995; MacGowan and Surdam, 1990; Barth, 1991; Lundegard and Kharaka, 1994; Strømgren et al., 1995; Amend et al., 1998; Utvik, 1999; Zeng and Liu, 2000; Franks et al., 2001; Varsányi et al., 2002; Zeng et al., 2002; Schulte and Shock, 2004; Veith et al., 2008; Ong et al., 2013; Glombitza et al., 2015; Zhu et al., 2015; Pizzarello and Shock, 2017; Konn et al., 2018).

At elevated temperatures and pressures, aqueous carboxylic acids decarboxylate, to form a hydrocarbon and carbon dioxide as in

$$\text{RCOOH (carboxylic acid)} \rightarrow \text{RH (hydrocarbon)} + CO_2, \tag{1}$$
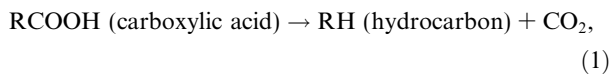
where R denotes a generic organic alkyl or aromatic group. Calculated equilibrium constants (K) consistent with reac-

tion (1) for several aqueous carboxylic acids are shown as functions of temperature at 1 kb in Fig. 1. The positive log K values indicate that decarboxylation products tend to be favored over the reactants, and that the drive for decarboxylation increases with increasing temperature. Note that at the temperature of the experiments described here, 300 °C, decarboxylation reactions for many alkanoic and aromatic acids have similar equilibrium constants, indicating that the product of the thermodynamic activities of aqueous CO_2 and hydrocarbons would exceed by $\sim10^3$ the activity of the aqueous acid at equilibrium. These results are consistent with the suggestion that elevated concentrations of carboxylic acids in natural solutions are preserved in metastable states relative to the decarboxylation reaction (Shock, 1988; 1989; 1994; Helgeson et al., 1993).

In the present study, we identify mechanisms of decarboxylation of carboxylic acids in water at high temperature and pressure by determining the rate constants for reaction of the model compound phenylacetic acid (PAA). PAA was selected for study because changes in the electronic properties of the aromatic ring lead to predictable thermodynamic and kinetic consequences that can reveal reaction mechanisms (Anslyn and Dougherty, 2006). As a result, reaction mechanisms can be deduced by studying how the rate of decarboxylation responds to different substituents on the aromatic ring. Analogous studies with the more geochemically abundant acetic acid are not possible. Another advantage of PAA is that the carbon atom bonded to the carboxyl group is a benzylic carbon that can stabilize ionic
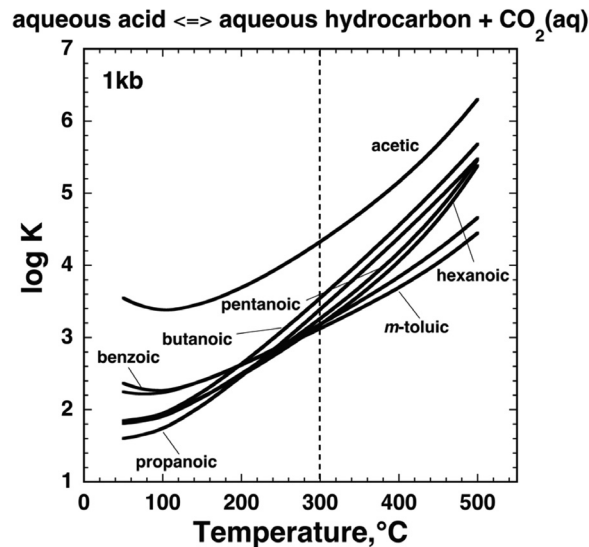

Fig. 1. Equilibrium constants for carboxylic acid decarboxylation consistent with reaction (1), at 1 kilobar and temperatures from 50 to 500 °C, calculated with standard state thermodynamic data for aqueous carboxylic acids from Shock (1995), aqueous CO_2 from Plyasunov and Shock (2001), and aqueous hydrocarbons from Shock and Helgeson (1990) or Plyasunov and Shock (2001). Note that log K values are all positive and become increasingly positive with increasing temperature, which reveals the underlying thermodynamic drive for organic acid decarboxylation at hydrothermal temperatures and pressures. Experiments in this study were conducted at 300 °C (vertical dashed line), where many log K values are similar for alkanoic and aromatic acids.

and radical reaction intermediates by resonance, resulting in faster reactions that are more compatible with the laboratory timescale. Furthermore, the product of decarboxylation of PAA is toluene, which is readily extracted into an organic solvent for quantitative analysis. Finally, other reactions that can compete with decarboxylation are largely eliminated owing to the inertness of the aromatic ring (McCollom et al., 2001). We reiterate that phenylacetic acid is being treated as a convenient and information-rich model to elucidate principles that may then be applied to more geochemically relevant compounds (see Section 5). Phenylacetic acid is not reported to be present in natural hydrothermal systems, although there are reports documenting its presence in groundwater (Cozzarelli et al., 1995; Schmitt et al., 1996; Thorn and Aiken, 1998; Di Gioia et al, 2001) where it may be consumed by microbes that produce toluene (Beller et al., 2018; Moe et al., 2018). The structures, names, and abbreviations of the PAAs studied here are given in Table 1. The sodium salt of phenylacetic acid, sodium phenylacetate, is abbreviated as Na-PA.

This study has four primary objectives: (1) to demonstrate the power of substituent effects in revealing fundamental details about geochemical decarboxylation reactions; (2) to determine how the rate constants and mechanisms of decarboxylation can be influenced by the speciation between carboxylic acid and carboxylate species; (3) to deduce the mechanisms of decarboxylation for phenylacetic acid and its carboxylate under hydrothermal conditions; and (4) to show how mechanistic information from a model system can lead to a more general understanding of decarboxylation in natural systems. This paper is one in a series of mechanistic studies of functional group chemistry in aqueous solutions at high temperatures and pressures (Yang et al., 2012; 2014; 2015; 2018; Shipp et al., 2013; 2014; Venturi et al., 2017; Bockisch et al., 2018; Robinson et al., 2019; Fecteau et al., 2019).
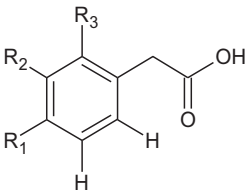
2. EXPERIMENTAL METHODS

Hydrothermal experiments were performed in gold (Au) capsule reactors (5 mm outer diameter × 0.127 mm wall thickness × 37.5 mm length, Au tubing from Depths of the Earth, Co.). The quoted purity of the Au tubing was 99.99% with impurities of Cu, Fe, or Ag of ≤50 ppm. Gold was used because previous work suggested that it is among the least active heterogeneous catalysts for acetic acid decarboxylation (Palmer and Drummond, 1986). The mechanical flexibility of Au allows the reaction vessels to

be pressurized significantly above the saturation pressure of water, eliminating the possibility of generating a vapor phase (if a vapor phase were present, there would be ambiguity as to whether decarboxylation occurred in the aqueous or vapor phase). Pre-cut Au tubes were cleaned by boiling in 12 M HCl for 30 min, rinsed three times with high-purity water (18.2 MΩ-cm), then annealed by heating at 600 °C for 12 h. Subsequently, one end of each tube was sealed by arc-welding, and the starting material (200 µmol) and Ar-sparged, high-purity water (200 µL) were loaded into each tube. Reagents were of the highest purity commercially available (see below) and used without further purification. The headspace of each Au capsule was purged with ultra-high purity (99.999%) argon for 2 min to minimize the amount of air in the capsule. Capsules were sealed by arc-welding without evaporative loss of water by submerging the closed end of the capsules into an H_2O-CH_3OH cold bath that had been chilled to a slurry using liquid N_2. The sealed capsules were tested for leaks prior to use by placing them in an oven at 110 °C for 10 min and checking for loss of mass.

A relatively high concentration of starting material (∼1 molal) was used to minimize errors in weighing and loading small quantities of the solid. Nevertheless, this quantity of PAA is soluble under the experimental conditions since PAA has an aqueous solubility of at least 1 m at 300 °C (PAA solubility is reported to increase from 0.130 m at 25 °C to 0.686 m at 86.7 °C; Morrison, 1944), consistent with the general trend of increasing organic compound solubility as water becomes a less polar solvent at higher temperatures (e.g., Price, 1981; Neely et al., 2008; Shock et al., 2013). The substituted PAAs are sufficiently similar to the parent (Table 1) that their solubilities should not be significantly different from that of PAA.

Gold capsules containing a phenylacetic acid and water were placed into a stainless-steel cold-seal pressure vessel (Williams et al., 2001). The vessel was pressurized with water and heated in a preheated furnace. Owing to the large heat capacity of the vessel, 2–3 h of heating was required to reach the experimental temperature of 300 °C. To avoid a temperature effect on the kinetic analysis owing to this slow heating, zero time ($t = 0$) for the experiments was defined as 2 h after the vessel was placed in the furnace. This means that there may be some product present at $t = 0$. The vessel was heated at 1034 bar (15,000 psi), which is similar to pressures at depths of several km in the Earth's crust, depending on the geological environment (i.e., lithostatic vs. hydrostatic pressure). Temperature was measured using a

Table 1
Ring-substituted phenylacetic acids studied in this work.

	R_1	R_2	R_3	Name of Compound	Abbreviation
	H	H	H	Phenylacetic acid	PAA
	CH$_3$	H	H	para-Methylphenylacetic acid	p-Me-PAA
	H	CH$_3$	H	meta-Methylphenylacetic acid	m-Me-PAA
	H	H	CH$_3$	ortho-Methylphenylacetic acid	o-Me-PAA
	F	H	H	para-Fluorophenylacetic acid	p-F-PAA
	H	F	H	meta-Fluorophenylacetic acid	m-F-PAA
	H	H	F	ortho-Fluorophenylacetic acid	o-F-PAA

corrosion-resistant thermocouple, and pressure was measured using a Bourdon gauge. The uncertainties are <5 °C in temperature and ±50 bar in pressure (Williams et al., 2001). Reactions were performed at 300 °C to expedite reaction rates, although it is understood that many diagenetic reactions of organic compounds occur at lower temperatures over longer durations (e.g., Tissot and Welte, 1984).

Experiments were performed at 300 °C and 1034 bar for various time periods (hours to days) to collect abundance versus time data. Once the desired time period was reached, the experiment was quenched by submerging the pressure vessel in a cold-water bath. The gold capsules were weighed to confirm that no leaks occurred during the experiment. Leak-free capsules were rinsed with methylene chloride (CH$_2$Cl$_2$) to remove any organic contaminants from the exterior of the capsule, and placed into 4 mL glass vials containing 3.0 mL of a solution of gas chromatography (GC) internal standards (see below). Capsules were opened while submerged in the CH$_2$Cl$_2$ solution by puncturing them with a rinsed blade. The vials were then capped and shaken to extract organic compounds into the CH$_2$Cl$_2$ phase. A stoichiometric excess of aqueous HCl was added to the vials to facilitate the recovery of the starting material, because the deprotonated carboxylate is too hydrophilic to be extracted into the organic solvent. It was found that the organic reactants and products are sufficiently hydrophobic that they can be analyzed by GC without prior derivatization.

Quantitative analysis was performed using a Varian CP-3800 gas chromatograph. Organic compounds were separated using a poly(5% diphenyl/95% dimethylsiloxane) column (Equity-5, Supelco, Inc.), and detected using a flame ionization detector. Organic products were identified using commercial standards, and quantities were determined using linear calibration curves that were referenced to internal standards. Initially, we used ethylbenzene (24.5 µmol per sample) as standard for both the reactant and products in experiments with m-Me-PAA, p-F-PAA, and o-F-PAA. We later switched to n-decane (15.4 µmol per sample) as standard for all organic products, as our group decided to adopt it as a uniform standard across several contemporaneous studies (Yang et al., 2012; Shipp et al., 2013; Bockisch et al., 2018; Fecteau et al., 2019). In the later experiments performed here, we used different PAAs (80 µmol per sample) as standards for other PAAs, as it was observed that their similar peak shapes gave the greatest reproducibility compared with the other standards. All of the standards were tested to ensure that the analyte and standard peaks did not overlap. A list of standards can be found in the Supplementary Online Materials (SOM). The GC conditions were as follows. The injector was set to 275 °C with a split ratio of 15. The oven temperature started at 40 °C with an immediate ramp of 10 °C/min to 140 °C; the heating rate was then decreased to 5 °C/min until the oven reached 220 °C, after which there was a final period of heating to 300 °C at a rate of 20 °C/min. The detector was kept at 300 °C throughout the analysis. Triplicate autosampler (Varian CP-8400) injections were performed to verify the reproducibility. Representative chromatograms for each experimental system are provided in the SOM. The material balance was computed from the number of moles of benzene rings in the reactant and products.

Materials and sources include: phenylacetic acid (Aldrich, 99%), p-methylphenylacetic acid (Alfa Aesar, 99%), m-methylphenylacetic acid (Alfa Aesar, 99%), o-methylphenylacetic acid (Aldrich, 99%), p-fluorophenylacetic acid (Alfa Aesar, 98%), m-fluorophenylacetic acid (Alfa Aesar, 98%), o-fluorophenylacetic acid (Alfa Aesar, >98%), methylene chloride (Fisher Scientific, 99.9%), n-decane (≥99%, Sigma-Aldrich), ethylbenzene (99.8%, Sigma-Aldrich), HCl (36% w/w aq. soln., Alfa Aesar), and NaOH (98%, Alfa Aesar). Sodium phenylacetates were prepared by neutralizing the appropriate PAA with NaOH solution and evaporating the mixture to dryness at 90 °C overnight. The purity of all starting materials was confirmed by GC analysis. Standards for decarboxylation products (i.e., toluenes and cresols) were purchased from Sigma-Aldrich or Alfa Aesar. High-purity water (18.2 MΩ-cm) was obtained from a Barnstead NANOpure DIamond water purification system.

3. RESULTS

3.1. Data and Observations

Analytical data from hydrothermal experiments with phenylacetic acid or sodium phenylacetate at 300 °C and 1034 bar are given in Table 2, and results for methyl- and fluoro-substituted phenylacetic acids and the corresponding sodium phenylacetates are given in Tables 3 and 4, respectively. Only methyl and fluoro substituents were used in this study because many other substituents traditionally used to probe reaction mechanisms (CH$_3$O—, NC—, and F$_3$C; e.g., Hammett, 1937) are incompatible with high-temperature water owing to hydrolysis at the substituent.

In all experiments, the amount of the reactant PAA or Na-PA decreased as a function of time, and the appropriately substituted toluene (R-PhCH$_3$, where Ph stands for the phenyl group or benzene ring) was the dominant or the only observed organic product. The mass balance was typically >90%. The major reaction, and often the only reaction, involved cleavage of the chemical bond between the benzylic and carboxyl carbons in the starting material. In the PAA experiments, the Au capsules were inflated after the experiments, and bubbling was observed after the capsules were punctured. This demonstrates that a gas was produced. Taken together, these observations imply that the PAAs reacted by decarboxylation as

$$\text{R-PhCH}_2\text{COOH(aq)} \rightarrow \text{R-PhCH}_3\text{(aq)} + \text{CO}_2\text{(aq)}, \qquad (2)$$

where the label (aq) indicates an aqueous species. In the Na-PA experiments, the Au capsules were not inflated after the experiments, and bubbling was not observed after the capsules were punctured. However, bubbles formed when aqueous HCl was added. This indicates that the capsules contained HCO$_3^-$, which reacted with the HCl to generate gaseous CO$_2$. The presence of bicarbonate and a toluene inside the capsules is indicative of decarboxylation at higher pH via
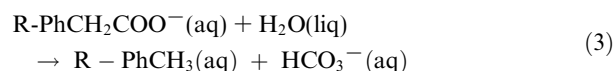
Table 2

Abundances of organic compounds from experiments with phenylacetic acid or sodium phenylacetate in water (200 μL) at 1034 bar in Au capsules. PAA and TOL stand for phenylacetic acid or sodium phenylacetate, and toluene, respectively. Analytical uncertainties in the initial amounts correspond to a weighing uncertainty of 0.3 mg, and uncertainties in the final amounts correspond to the standard deviation from three gas chromatograph injections.

Temp. (°C)	Duration (h)	Initial PAA (μmol)	Final PAA (μmol)	Final TOL (μmol)	Material balance (%)[a]
Phenylacetic acid					
298	2	203 ± 2	185 ± 2	15.4 ± 0.1	99 ± 1
300	6	209 ± 2	153 ± 3	41.9 ± 0.2	93 ± 2
302	11	220 ± 2	137 ± 4	83.2 ± 0.3	100 ± 2
299	16	212 ± 2	118 ± 3	88.1 ± 0.8	97 ± 2
300	18.7	202 ± 2	81 ± 2	117.7 ± 0.8	98 ± 1
302	23	211 ± 2	66 ± 4	140.2 ± 0.1	98 ± 2
301[b]	23	204 ± 2	66 ± 2	132.9 ± 0.6	97 ± 1
301	23	203 ± 2	77.5 ± 0.3	122.6 ± 0.4	98 ± 1
301	29	209 ± 2	59 ± 3	148 ± 1	99 ± 2
300	40.1	212 ± 2	42 ± 2	166.2 ± 0.5	98 ± 1
301	50	207 ± 2	22.1 ± 0.3	179.7 ± 0.8	97 ± 1
300	55.6	203 ± 2	13.9 ± 0.5	175.8 ± 0.5	93 ± 1
300	72.5	205 ± 2	10 ± 2	201 ± 3	103 ± 2
Phenylacetic acid + 707 mg Au					
301[b]	23	206 ± 2	72 ± 4	136.8 ± 0.8	101 ± 2
Sodium phenylacetate					
297	0	208 ± 2	185 ± 2	13.1 ± 0.2	96 ± 1
299	2	202 ± 2	150 ± 2	54.5 ± 0.1	101 ± 1
301	6	202 ± 2	78 ± 3	123 ± 1	100 ± 2
301[c]	6	205 ± 2	89 ± 1	110 ± 1	97 ± 1
301	6	210 ± 2	72 ± 2	131 ± 2	97 ± 2
300	12.2	200 ± 2	29 ± 3	160 ± 3	94 ± 2
301	16	200 ± 2	7.8 ± 0.1	181 ± 2	95 ± 1
302	23	207 ± 2	2.9 ± 0.1	197.8 ± 0.6	97.0 ± 0.9
Sodium phenylacetate + 648 mg Au					
301[c]	6	200 ± 2	93.2 ± 0.4	105 ± 5	99 ± 3

[a] The material balance was computed based on the number of moles of benzene rings in the reactant and organic product.
[b,c] These experiments were performed in the same run to ensure optimal comparability.

$$R\text{-}PhCH_2COO^-(aq) + H_2O(liq)$$
$$\rightarrow R - PhCH_3(aq) + HCO_3^-(aq) \qquad (3)$$

Small quantities of cresols (*i.e.*, hydroxytoluenes) were detected in the experiments with fluorinated reactants (Table 4). As shown in reaction scheme (4), cresols can be produced by (**I**) hydrolysis of the F-PAA, followed by decarboxylation of the hydroxyphenylacetic acid (HO-PAA); or (**II**) decarboxylation of the F-PAA, followed by hydrolysis of the fluorotoluene
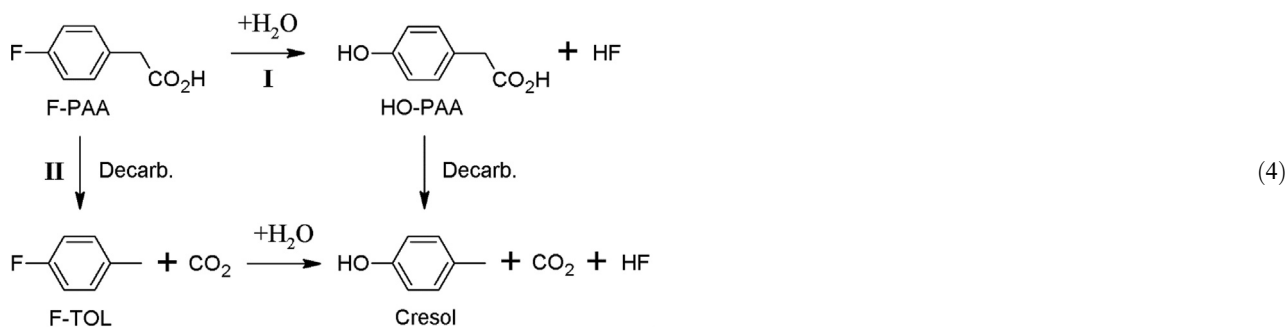

$$(4)$$

Table 3
Abundances of organic compounds from experiments with ring-methylated phenylacetic acids or sodium phenylacetates in water (200 μL) at
1034 bar in Au capsules. PAA and TOL stand for the appropriate substituted phenylacetic acid or sodium phenylacetate, and toluene,
respectively (the starting stereochemistry is preserved); and ND means not detected (<0.1 μmol). Analytical uncertainties in the initial
amounts correspond to a weighing uncertainty of 0.3 mg, and uncertainties in the final amounts correspond to the standard deviation from
three gas chromatograph injections.

Temp. (°C)	Duration (h)	Initial PAA (μmol)	Final PAA (μmol)	Final TOL (μmol)	Material Balance (%)[a]
p-Methylphenylacetic acid					
299	2	206 ± 2	195 ± 1	11.95 ± 0.03	101 ± 1
300	12.9	209 ± 2	143.1 ± 0.2	61.8 ± 0.1	98.2 ± 0.9
302	23	205 ± 2	104 ± 3	99.5 ± 0.3	99 ± 2
300	23	202 ± 2	104 ± 1	95.7 ± 0.1	99 ± 1
300	52.8	207 ± 2	51 ± 5	156.4 ± 0.8	100 ± 2
Sodium p-methylphenylacetate					
298	2	198 ± 2	186 ± 2	9.23 ± 0.06	99 ± 1
300	6	204 ± 2	174 ± 2	31.6 ± 0.2	101 ± 1
300	23	204 ± 2	99 ± 2	104.5 ± 0.3	99 ± 1
300	23	204 ± 2	80.1 ± 0.2	115.9 ± 0.3	96.3 ± 0.8
300	52.5	205 ± 2	37.1 ± 0.6	158.9 ± 0.7	95.7 ± 0.9
m-Methylphenylacetic acid					
296	0	202 ± 2	169.4 ± 0.5	35.4 ± 0.1	101 ± 1
300	2	199 ± 2	72 ± 5	127.9 ± 0.4	100 ± 3
299	4	210 ± 2	42 ± 2	169.9 ± 0.1	101 ± 1
300	9	202 ± 2	4.6 ± 0.1	194.8 ± 0.5	99 ± 1
300	23	197 ± 2	ND	184.9 ± 0.2	94 ± 1
Sodium m-methylphenylacetate					
300	2	202 ± 2	144 ± 3	56.4 ± 0.9	99 ± 2
300	6	208 ± 2	107.2 ± 0.3	97.9 ± 0.4	98.4 ± 0.9
300	14	203 ± 2	58 ± 1	139.3 ± 0.3	97 ± 1
300	23	213 ± 2	21.9 ± 0.8	182.5 ± 0.5	95.8 ± 0.9
o-Methylphenylacetic acid					
300	2	206 ± 2	170 ± 3	33.0 ± 0.1	98 ± 2
300	5	211 ± 2	152 ± 1	54.7 ± 0.4	98 ± 1
301	7.5	205 ± 2	95 ± 5	100.9 ± 0.1	96 ± 3
301	15.5	197 ± 2	65 ± 4	125.7 ± 0.7	97 ± 3
300	23	207 ± 2	34 ± 1	166.5 ± 0.2	97 ± 1
300	23	203 ± 2	34.3 ± 0.1	164 ± 1	98 ± 1
300	31	201 ± 2	7.9 ± 0.2	179.7 ± 0.5	93 ± 1
Sodium o-methylphenylacetate					
296	0	208 ± 2	192 ± 3	17.3 ± 0.2	101 ± 2
300	2	207 ± 2	111.7 ± 0.4	96.8 ± 0.6	100.8 ± 0.9
301	3.5	199 ± 2	97.3 ± 0.7	100.7 ± 0.7	99 ± 1
300	6	218 ± 2	49.0 ± 0.8	162 ± 1	97 ± 1

[a] The material balance was computed based on the number of moles of benzene rings in the reactant and organic product.

Insufficient information is available from the experiments to distinguish between these possibilities, but because cresols are minor products, it is not necessary to know their mechanisms of formation to quantify the kinetics of the decarboxylation reaction (see Section 3.2). Yet, it is notable that cresols formed faster in experiments with Na-F-PAs than in those with F-PAAs (Table 4), suggesting that the mechanism of cresol formation depends on speciation and/or pH.

We focused on measuring the primary organic products rather than the amount of CO_2 formed by decarboxylation because CO_2 is not amenable to our analytical procedure. Small amounts (<10–20 μmol) of unidentified products could also have formed, and appear to be partly responsible for mass balance deficits in experiments where the mass balance decreases monotonically with time (e.g., p-F-PAA, o-F-PAA; Table 4). In the latter two cases, we

inspected closely the longest-duration chromatograms shown in the SOM, and found several minor peaks. They include trace toluene (<1 μmol), a likely one-ring compound with a retention time of ~6.5 min, and what may be various two-ring compounds with retention times between ~15 and 20 min. Semi-quantitative analysis based on peak area ratios relative to the ethylbenzene internal standard that was used in these experiments suggests that these products contain ~11 μmol of phenyl equivalents from the 526 h p-F-PAA experiment, and ~7 μmol of phenyl equivalents from the 265.67 h o-F-PAA experiment. Including these amounts in the mass balances would increase them to ~99% and ~95%, respectively. However, even if a minor mass balance deficit persists, it would not alter our conclusions on the values of decarboxylation rate constants (see uncertainty analysis in Section 3.2).

Table 4

Abundances of organic compounds from experiments with ring-fluorinated phenylacetic acids or sodium phenylacetates in water (200 μL) at 1034 bar in Au capsules. PAA, TOL, and CRE stand for the appropriate substituted phenylacetic acid or sodium phenylacetate, toluene, and cresol, respectively (the starting stereochemistry is preserved); and ND means not detected (<0.1 μmol). Analytical uncertainties in the initial amounts correspond to a weighing uncertainty of 0.3 mg, and uncertainties in the final amounts correspond to the standard deviation from three gas chromatograph injections.

Temp. (°C)	Duration (h)	Initial PAA (μmol)	Final PAA (μmol)	Final TOL (μmol)	Final CRE (μmol)	Material balance (%)[a]
p-Fluorophenylacetic acid						
300	2	213 ± 2	211 ± 5	1.49 ± 0.03	ND	100 ± 3
301	23	204 ± 2	185 ± 5	11.5 ± 0.2	0.54 ± 0.04	97 ± 3
300	23	199 ± 2	183.4 ± 0.2	12.3 ± 0.1	0.48 ± 0.01	99 ± 1
299	167	204 ± 2	121 ± 2	71.4 ± 0.3	4.51 ± 0.08	96 ± 1
299	526	202 ± 2	46.2 ± 0.7	134.9 ± 0.4	8.7 ± 0.1	94 ± 1
Sodium *p*-fluorophenylacetate						
300	2	195 ± 2	164 ± 2	24.2 ± 0.3	3.0 ± 0.3	98 ± 2
300	6	206 ± 2	135 ± 1	54.2 ± 0.4	12.8 ± 0.3	98 ± 1
302	15	203 ± 2	67.0 ± 0.1	96 ± 1	27.3 ± 0.6	94 ± 1
300	23.03	202 ± 2	43.3 ± 0.4	107.8 ± 0.7	39 ± 3	94 ± 2
300	31.5	198 ± 2	24.2 ± 0.6	116 ± 1	43.8 ± 0.4	93 ± 1
m-Fluorophenylacetic acid						
301	2	204 ± 2	169 ± 1	32.7 ± 0.4	ND	99 ± 1
299	5	211 ± 2	138 ± 2	67.9 ± 0.4	0.6 ± 0.1	98 ± 1
300	12.2	203 ± 2	94 ± 2	106.5 ± 0.4	1.4 ± 0.1	99 ± 2
301	16	198 ± 2	54.5 ± 0.6	137 ± 1	2.32 ± 0.03	98 ± 1
301	23	204 ± 2	32 ± 3	161 ± 2	3.6 ± 0.2	97 ± 2
300	32.5	204 ± 2	20 ± 1	176 ± 4	3.2 ± 0.1	97 ± 2
Sodium *m*-fluorophenylacetate						
296	0	206 ± 2	123.7 ± 0.4	73 ± 3	3.0 ± 0.5	97 ± 2
299	0.5	210 ± 2	66 ± 2	133 ± 4	8 ± 1	98 ± 3
298	1	207 ± 2	48.0 ± 0.5	140 ± 1	10.4 ± 0.1	96 ± 1
300	2	209 ± 2	12.4 ± 0.1	167 ± 2	18.1 ± 0.2	94 ± 1
300	6	203 ± 2	ND	149 ± 2	38.7 ± 0.7	92 ± 1
o-Fluorophenylacetic acid						
301	2	207 ± 2	198 ± 4	3.74 ± 0.05	ND	98 ± 2
300	23	206 ± 2	166.1 ± 0.1	24.7 ± 0.1	2.16 ± 0.02	93.9 ± 0.9
300	97	202 ± 2	107 ± 5	74.7 ± 0.4	12.6 ± 0.3	96 ± 3
299	265.67	205 ± 2	36 ± 2	125 ± 1	26.3 ± 0.6	91 ± 1
Sodium *o*-fluorophenylacetate						
297	0	209 ± 2	86 ± 1	97 ± 1	2.02 ± 0.06	88 ± 1
297	0	205 ± 2	90.1 ± 0.2	88.1 ± 0.2	1.76 ± 0.05	87.8 ± 0.7
300	0.75	206 ± 2	28.0 ± 0.2	144.0 ± 0.7	7.71 ± 0.04	87.1 ± 0.8
298	1	194 ± 2	30.4 ± 0.2	144.9 ± 0.4	7.6 ± 0.1	94.5 ± 0.9
300	2	202 ± 2	6.1 ± 0.1	159.0 ± 0.8	18.3 ± 0.3	90.8 ± 2
300	6	205 ± 2	ND	161 ± 1	33.9 ± 0.4	95 ± 1

[a] The material balance was computed based on the number of moles of benzene rings in the reactant and organic products.

A potential concern is whether the walls of the Au capsules catalyze decarboxylation. To explore this possibility, experiments were performed in which small pieces of Au tubing were added to capsules containing PAA or Na-PA. After 23 h at 301 °C and 1034 bar, the conversion of PAA was 66 ± 1%, and that of PAA with the additional Au pieces was 66 ± 1% (Table 2). After 6 h at 301 °C and 1034 bar, the conversion of Na-PA was 55 ± 1%, and that of Na-PA with extra Au was 53 ± 1% (Table 2). These results allow the conclusion that Au does not affect the decarboxylation of PAA and Na-PA under the present experimental conditions.

Triplicate experiments were performed for both PAA and Na-PA, and duplicate experiments were performed for *p*-Me-PAA, Na-*p*-Me-PA, *o*-Me-PAA, *p*-F-PAA, and Na-*o*-

F-PA to determine the reproducibility between experiments (Tables 2–4). The percent yield in most replicate experiments were within a few percent, while a few exhibited discrepancies of 5–10%. Based on these comparisons, a median value of 3% was adopted for the absolute uncertainty in the percent yields for all the experimental data. This uncertainty in the analytical data contributes to the estimated uncertainties in the reaction rate constants as described next.

3.2. Kinetic analysis

The kinetics of the disappearance of PAAs and Na-PAs can be determined by plotting the percent yield of the unreacted starting material and the percent yield of the organic products as functions of time, as shown in Fig. 2 for PAA
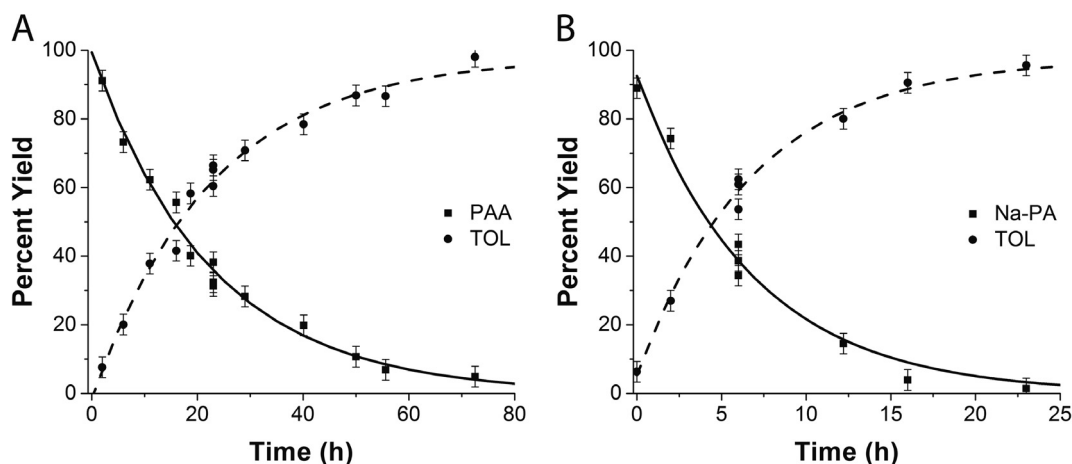
Fig. 2. Percent yields of organic compounds as functions of time from experiments in water at 300 °C and 1034 bar. (A) PAA and toluene (TOL) from experiments with PAA; and (B) Na-PA and TOL from experiments with Na-PA. In all experiments the concentration of the starting material was ~1 m. A 3% uncertainty in yields was assigned based on an analysis of replicates in the entire dataset. First-order kinetic curves were drawn by performing least squares regression, resulting in solid curves for reactants and dashed curves for products. Note differences in overall duration of experiments.

and Na-PA, and in Figs. 3 and 4 for ring-methylated and ring-fluorinated acids and carboxylates, respectively. The results in Fig. 2 show that reactions were allowed to proceed to high conversion (>70%), to yield tight constraints on kinetic models. All results are consistent with progress toward ratios among the reactant and products consistent with equilibrium constants similar to those shown in Fig. 1, but the durations of the experiments were insufficient for those states to be reached. Note that some of the reactants (i.e., m-Me-PAA in Fig. 3, Na-m-F-PA and Na-o-F-PA in Fig. 4) became undetectable after sufficient durations (Tables 3 and 4). Evidently, the decarboxylation of PAAs and Na-PAs is irreversible (i.e., the products of decarboxylation are much more energetically stable than the reactant) at these experimental conditions, consistent with prior thermodynamic evaluations (Shock, 1988; 1989; 1994). The apparent irreversibility of decarboxylation distinguishes it from functional group transformations that do not involve the breaking of carbon-carbon bonds (e.g., alkane-alkene, alcohol-alkene, alcohol-ketone interconversions), which can reach metastable equilibrium states (Seewald, 1994; Yang et al., 2012; Shipp et al., 2013; 2014; Bockisch et al., 2018). The decarbonylation of dibenzyl ketone is another reaction that behaves irreversibly under hydrothermal conditions, and also involves carbon-carbon bond cleavage (Yang et al., 2012).

To derive reaction rate constants, the experimental data were normalized in terms of the yield, calculated from data in Tables 2–4 as the number of moles of the organic compound of interest divided by the number of moles of the starting material (based on conservation of unreactive aromatic rings). Note that here we use the term yield as a general variable for both the reactant and products. Yield is preferable to concentration as a kinetic variable in this case, because the concentration of the starting material varied slightly among the experiments owing to slight differences in the weighed mass of the starting material. Data regression used the first-order integrated rate equations

$$Y_{PA} = (Y_{PA})_{t=0} e^{-k_{app}t}, \tag{5a}$$

and

$$Y_{OP} = (Y_{OP})_{t=0} + (Y_{PA})_{t=0}(1 - e^{-k_{app}t}), \tag{5b}$$

where Y_{PA} stands for the yield of phenylacetate species (i.e., acid + carboxylate), Y_{OP} represents the yield of organic products, k_{app} is the apparent first-order rate constant for the disappearance of the starting material, and t corresponds to time. The analytical method quantifies total phenylacetate as the carboxylate is converted to the acid form during sample workup prior to GC analysis. The curves shown in Figs. 2–4 and corresponding values of k_{app} were obtained by simultaneously fitting all Y_{PA} and Y_{OP} values in each figure panel to Eqs. (5a) and (5b). The plots in Figs. 2–4 reveal that first-order kinetics provide a close representation of the experimental data. The standard error in k_{app} was computed to be ~5%. However, when we overlaid curves with manually adjusted values of k_{app} onto the plots and compared them to the error bars for each point that were determined from replicate experiments (see Section 3.1), we observed that a wider range of k_{app} values show acceptable consistency with the data. Because the standard error seems too small relative to the variability that is expected based on our experience of performing these experiments, we consider the more conservative ranges in k_{app} that were estimated from the above graphical analysis to provide more realistic representations of the uncertainty in the rate constants.

We calculate the rate constants for decarboxylation (k_{decarb}; Table 5) from k_{app} based on the product distributions. In systems with a substituted toluene as the only organic product and a high mass balance, $k_{app} = k_{decarb}$ based on Eqs. (5a) and (5b). These criteria are satisfied by the parent and methyl-substituted systems (Figs. 2 and 3). The fluoro-substituted systems (Fig. 4) are more complicated because cresols are also produced. If cresols are produced solely by the hydrolysis of fluorotoluenes, then
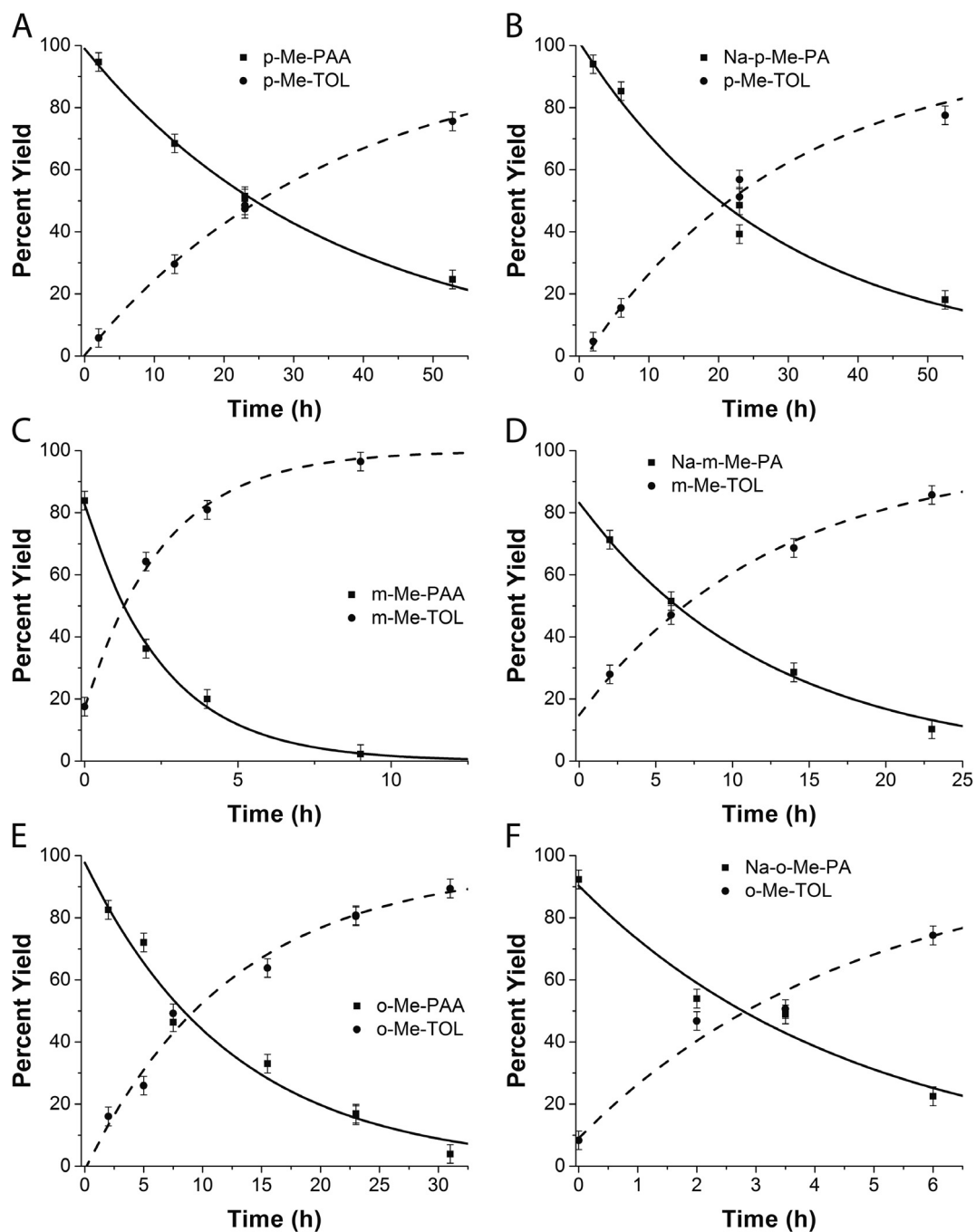
Fig. 3. Percent yields of organic compounds as functions of time from experiments with ring-methylated phenylacetic acids or sodium phenylacetates in water at 300 °C and 1034 bar. (A) *para*-Methylphenylacetic acid (*p*-Me-PAA) and *para*-methyltoluene (*p*-Me-TOL) from experiments with *p*-Me-PAA; (B) sodium *para*-methylphenylacetate (Na-*p*-Me-PA) and *p*-Me-TOL from experiments with Na-*p*-Me-PA; (C) *meta*-methylphenylacetic acid (*m*-Me-PAA) and *meta*-methyltoluene (*m*-Me-TOL) from experiments with *m*-Me-PAA; (D) sodium *meta*-methylphenylacetate (Na-*m*-Me-PA) and *m*-Me-TOL from experiments with Na-*m*-Me-PA; (E) *ortho*-methylphenylacetic acid (*o*-Me-PAA) and *ortho*-methyltoluene (*o*-Me-TOL) from experiments with *o*-Me-PAA; and (F) sodium *ortho*-methylphenylacetate (Na-*o*-Me-PA) and *o*-Me-TOL from experiments with Na-*o*-Me-PA. The concentration of the starting material was ~1 m in each case. A 3% uncertainty in yields was assigned based on an analysis of replicates in the entire dataset. First-order kinetic curves were drawn by performing least squares regression, resulting in solid curves for reactants and dashed curves for products. Note the differing horizontal axes reflecting differences in overall experimental durations.

$k_{app} = k_{decarb}$. In this case (pathway II in scheme (4)), organic products in Eq. (5b) correspond to the sum of the appropriate fluorotoluene and cresol. In the alternative endmember, it is assumed that cresols form via pathway I in scheme (4) that is competitive with decarboxylation of F-PAAs. This would imply that $k_{app} = k_{decarb} + k_{hydro}$,
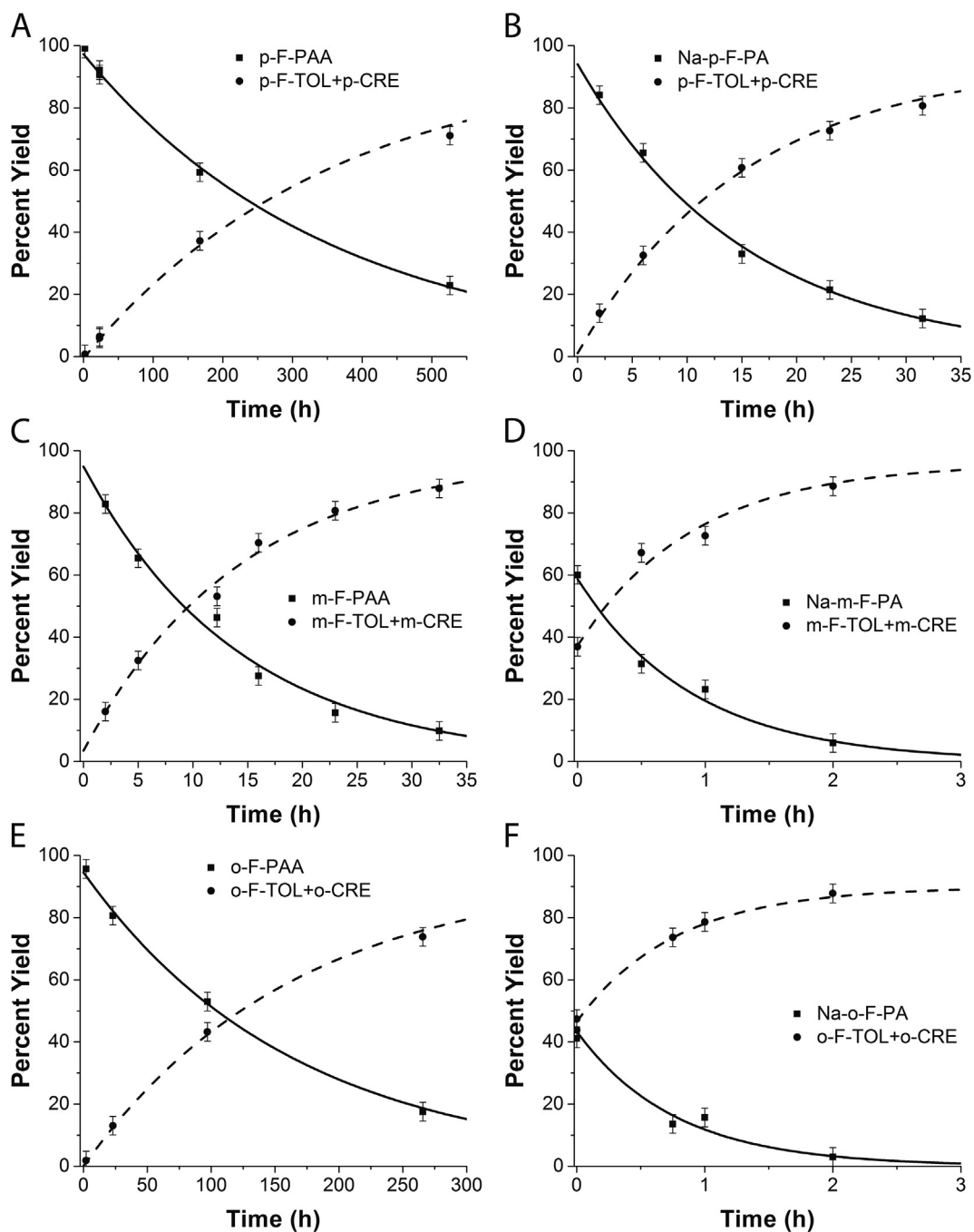
Fig. 4. Percent yields of organic compounds as functions of time from experiments with ring-fluorinated phenylacetic acids or sodium phenylacetates in water at 300 °C and 1034 bar. (A) *para*-Fluorophenylacetic acid (*p*-F-PAA) and *para*-fluorotoluene (*p*-F-TOL) + *para*-cresol (*p*-CRE) from experiments with *p*-F-PAA; (B) sodium *para*-fluorophenylacetate (Na-*p*-F-PA) and *p*-F-TOL + *p*-CRE from experiments with Na-*p*-F-PA; (C) *meta*-fluorophenylacetic acid (*m*-F-PAA) and *meta*-fluorotoluene (*m*-F-TOL) + *meta*-cresol (*m*-CRE) from experiments with *m*-F-PAA; (D) sodium *meta*-fluorophenylacetate (Na-*m*-F-PA) and *m*-F-TOL + *m*-CRE from experiments with Na-*m*-F-PA; (E) *ortho*-fluorophenylacetic acid (*o*-F-PAA) and *ortho*-fluorotoluene (*o*-F-TOL) + *ortho*-cresol (*o*-CRE) from experiments with *o*-F-PAA; and (F) sodium *ortho*-fluorophenylacetate (Na-*o*-F-PA) and *o*-F-TOL + *o*-CRE from experiments with Na-*o*-F-PA. In all experiments the concentration of the starting material was ∼ 1 m. A 3% uncertainty in yields was assigned based on an analysis of replicates in the entire dataset. First-order kinetic curves were drawn by performing least squares regression, reflected in the solid curves for reactants and dashed curves for products. The dashed curves through the products shown here are consistent with the formation of cresols via pathway II in scheme (4). However, the determination of decarboxylation rate constants does not depend strongly on the specific pathway of cresol formation (see text). Note differences in overall duration of experiments.

Table 5

First-order rate constants (k_{decarb}) for the decarboxylation of phenylacetic acids and sodium phenylacetates in water at 300 °C and 1034 bar, and Hammett substituent parameters (σ) used in this work. The uncertainties were estimated by graphical analysis as described in Section 3.2. See Table 1 for definitions of the abbreviated names.

Reactant	σ^a	$100 \times k_{decarb}$ (h^{-1})
Phenylacetic Acids		
PAA	0[b]	4.4 ± 0.5
p-Me-PAA	-0.07[c]	2.8 ± 0.4
m-Me-PAA	-0.31[d]	39 ± 6
o-Me-PAA	-0.07[c]	8 ± 2
p-F-PAA	0.34[c]	0.27 ± 0.03
m-F-PAA	-0.07[d]	7 ± 1
o-F-PAA	0.34[c]	0.55 ± 0.07
Sodium Phenylacetates		
Na-PA	0[b]	14.5 ± 2
Na-p-Me-PA	-0.17[e]	3.5 ± 0.7
Na-m-Me-PA	-0.07[c]	8 ± 1.5
Na-o-Me-PA	-0.17[e]	21 ± 5
Na-p-F-PA	-0.03[e]	5.5 ± 1
Na-m-F-PA	0.34[c]	105 ± 20
Na-o-F-PA	-0.03[e]	125 ± 30

[a] All σ values from Hansch et al. (1991).
[b] Zero by convention.
[c] σ_m.
[d] σ_p^+.
[e] σ_p^-.

where k_{hydro} refers to the rate constant for the hydrolysis of the fluorinated PAA or Na-PA. The integrated rate equations for this scenario are

$$Y_{F\text{-}PA} = (Y_{F\text{-}PA})_{t=0}e^{-k_{app}t}, \tag{6a}$$

and

$$Y_{F\text{-}TOL} = (Y_{F\text{-}TOL})_{t=0}$$
$$+ (k_{decarb}/k_{app})(Y_{F\text{-}PA})_{t=0}(1 - e^{-k_{app}t}). \tag{6b}$$

The ranges of k_{decarb} reported in Table 5 for the F-PAAs and Na-F-PAs were determined by performing non-linear regressions for both endmember cases of cresol formation (using either Eqs. (5a) and (5b), or Eqs. (6a) and (6b)), as well as accounting for uncertainties that are inherent to the experiments by graphical analysis (see above). We find that k_{decarb} could be ~5–30% smaller than k_{app}, essentially because the yields of the cresols are low compared with those of the toluenes.

4. DISCUSSION

4.1. Probing mechanisms with substituent effects

The mechanisms of decarboxylation can be probed by assessing the effects of substituents on the rate constant (k) of the reaction (e.g., Hammett, 1937; Johnson, 1973). Substituent effects are quantified using the Hammett equation, which is an example of a linear free energy relationship originally obtained for equilibrium constants (Anslyn and Dougherty, 2006), and which can be expressed for rate constants as

$$\log(k) = \sigma \cdot \rho + b \tag{7}$$

where ρ indicates a constant that is characteristic of the reaction mechanism, solvent, temperature, and pressure; σ stands for a substituent parameter that depends upon the identity and position of the substituent on the benzene ring; and b designates a constant intercept that is ideally the value of $\log(k)$ for the unsubstituted structure; i.e., for which σ is zero[1]. Electron-withdrawing substituents increase the acidity of benzoic acid and so they have positive values of σ. The opposite is true for electron-donating substituents. There are also specialized σ scales for different kinds of reactions for which benzoic acid dissociation may not be the best reference. In particular, the σ^+ and σ^- scales are designed to account for substituents that directly stabilize or destabilize positive or negative charges in benzene rings by resonance effects. As discussed below, the σ^+ and σ^- scales are relevant in the present work.

The ρ parameter obtained from a Hammett analysis indicates how sensitive the rate constant is to substituents. Its magnitude, and in particular its sign, can be used to infer details of how bonds are broken and/or formed in the reaction. The sign of ρ reflects changes in charge build-up in or near the benzene ring in the transition state of the reaction. In general, when $\rho > 0$, negative charge is increasing (or positive charge is decreasing) in the benzene ring in the transition state, and when $\rho < 0$, positive charge is increasing (or negative charge is decreasing) in the benzene ring in the transition state (Anslyn and Dougherty, 2006).

The Hammett plots shown in Fig. 5 were used to determine experimental values of ρ for decarboxylation of PAAs and Na-PAs in water at 300 °C and 1034 bar, using substituent constants from Hansch et al. (1991) and rate constants for decarboxylation from Table 5. For decarboxylation of the PAAs, it was found that electron-donating substituents accelerated the reaction whereas electron-withdrawing substituents slowed the reaction. In the case of decarboxylation of the Na-PAs, however, the opposite trend was observed; i.e., electron-donating substituents slowed the reaction whereas electron-withdrawing substituents accelerated it. For both the PAAs and the Na-PAs, we found that plots with the simple σ scale exhibited much weaker linear correlations than plots that used the σ^+ or σ^- scales as appropriate.

The definition of ortho-, meta-, and para- in the context of the σ values requires some clarification. As discussed in more detail below, the substituent effects for the PAAs suggest that positive charge is formed on the benzene ring in the transition state, resulting from protonation of the ring, as indicated by

---

[1] The reference reaction for the Hammett equation, for which ρ is arbitrarily set to unity, is the dissociation of substituted benzoic acids in water at 25 °C and 1 bar. Measured values of the dissociation constants for variously substituted benzoic acids are used to define values for σ_m (i.e., for a substituent in the meta-position of a benzene ring) and σ_p (i.e., for a substituent in the para-position of a benzene ring) from the appropriate pK_a values. Substituent effects in the ortho-position are often not considered reliable due to steric effects that cannot be generalized to different reactions (Gould, 1959).
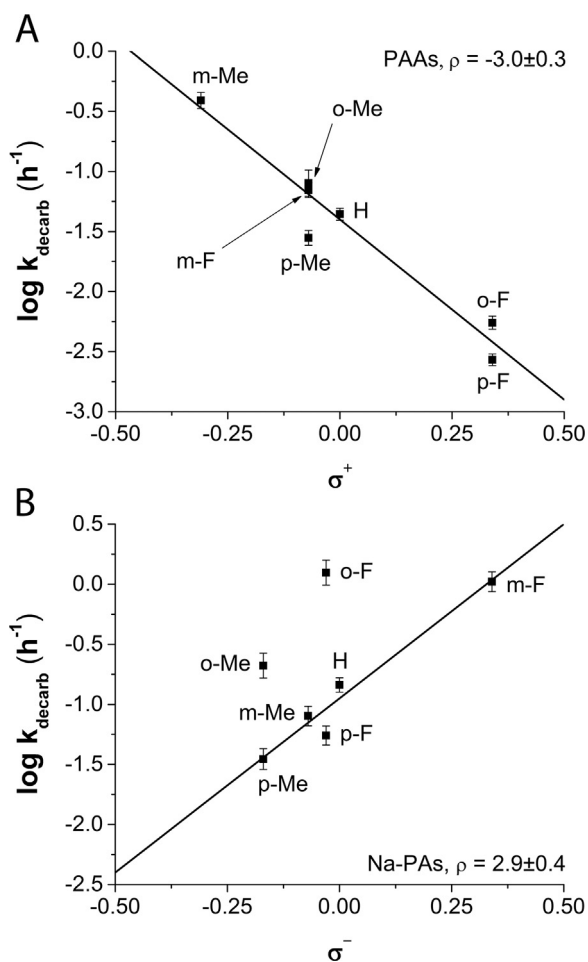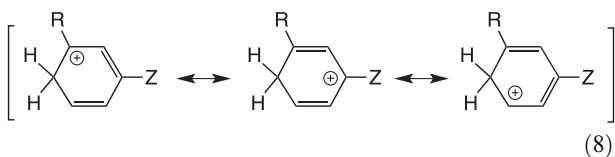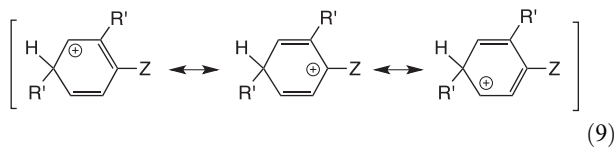
be minimal steric effects since the substituent is *ortho*- to a carbon that carries only two hydrogens. The resonance electronic effects should be properly described by σ_p^+. On the other hand, substituents in the *ortho*- or *para*-positions with respect to the acid, indicated as R' in

$$\left[\begin{array}{ccc} & \text{R'} & \text{R'} & \text{R'} \\ \text{H} \oplus \text{---Z} & \longleftrightarrow & \text{H} \quad \oplus \text{---Z} & \longleftrightarrow & \text{H} \quad \text{---Z} \\ \text{R'} & \text{R'} & \text{R'} \oplus \end{array} \right] \tag{9}$$

cannot directly influence the positive charge by resonance, since the charge is not delocalized onto any of these carbon atoms. Therefore, substituents in these positions are better described with σ_m, which is the appropriate parameter for substituents that are bonded to a carbon that is *adjacent* to the carbon that carries the charge. Using the substituent parameters in this way gives a strong linear correlation with a negative slope, as shown in Fig. 5A, consistent with formation of a positive charge over the course of the reaction mechanism indicated in schemes (8) and (9).

As discussed further below, the substituent effects for the carboxylate salts are consistent with formation of negative charge on the ring, of the kinds indicated in

$$\begin{array}{l} \text{A} \left[\begin{array}{ccc} \text{R} & \text{R} & \text{R} \\ \text{R---} \ominus \text{==} & \longleftrightarrow & \text{R---} \ominus \text{==} & \longleftrightarrow & \text{R---} \text{==} \\ & & & & \ominus \end{array} \right] \\[2em] \text{B} \left[\begin{array}{ccc} \text{R'} & \text{R'} & \text{R'} \\ \ominus \text{==} & \longleftrightarrow & \ominus \text{==} & \longleftrightarrow & \text{==} \\ & & & & \ominus \end{array} \right]. \end{array} \tag{10}$$

Substituents R in the positions shown in scheme (10)A, *i.e.*, in the *ortho*- and *para*-positions with respect to the (former) acid group, can directly stabilize or destabilize the negative charge in the ring by resonance. The influence of these substituents is therefore best described using σ^-. However, R' substituents in the position shown in scheme (10)B, *i.e.*, *meta*-to the (former) acid, cannot directly influence the negative charge. The influences of these substituents, therefore, are better described with σ_m. The Hammett plot for the Na-PAs constructed using these substituent values (Fig. 5B) exhibits a strong linear correlation with a positive slope, except for structures with *ortho*-substituents, which were excluded from the fitting procedure because *ortho* effects generally have a significant steric component that cannot be captured by a single parameter (Anslyn and Dougherty, 2006). Consequently, there is no universal set of Hammett parameters for *ortho* substituents. As discussed above, we chose to assign *para* σ^- parameters to both the *para* and *ortho* substituents to capture resonance effects that are expected to be similar at these two positions, and we included *ortho*-substituted systems in Fig. 5B so that any discrepancies between *ortho* and *para* can be readily identified, which may provide information about steric and inductive effects that are secondary to the overall behavior of the correlation. Outliers in the Hammett plots are discussed in Section 4.2.2.

Fig. 5. Hammett plots for the decarboxylation of (A) phenylacetic acids and (B) sodium phenylacetates in water at 300 °C and 1034 bar. Logarithms of rate constants for decarboxylation are plotted as a function of the Hammett resonance-based substituent parameter σ^+ or σ^- using values from Table 5. The lines provide the closest linear fits to the data. The Hammett reaction constant ρ corresponds to the slope, and its uncertainty is expressed as the standard error.

$$\left[\begin{array}{ccc} \text{R} & \text{R} & \text{R} \\ \text{H} \oplus \text{---Z} & \longleftrightarrow & \text{H} \quad \oplus \text{---Z} & \longleftrightarrow & \text{H} \quad \text{---Z} \\ \text{H} & \text{H} & \text{H} \oplus \end{array} \right] \tag{8}$$
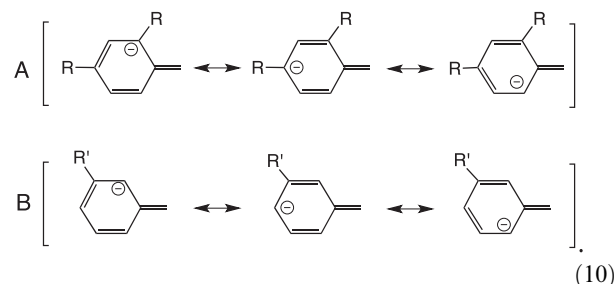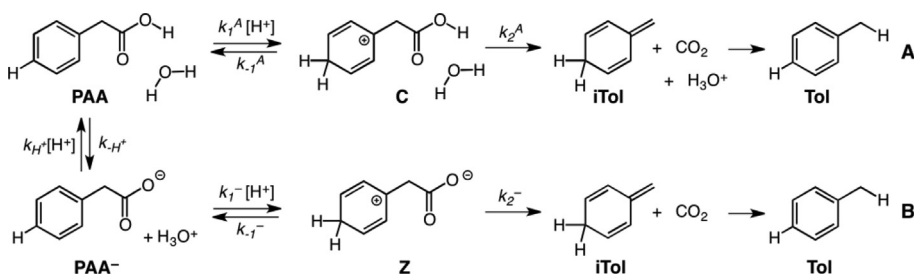
where Z represents the acetic group. An electron-donating substituent, R, in the position shown in scheme (8) will stabilize the positive charge via resonance effects. The substituent is in the *meta*-position with respect to the acetic group, but it is in the *ortho*-position with respect to the site of protonation of the ring, which is responsible for generating the positive charge. Therefore, it is expected that σ^+ should describe substituent effects for PAAs substituted in this position. Each of the R substituents in these positions were assigned the appropriate σ^+ value for the *para*-position (*i.e.*, σ_p^+) since *ortho*-specific σ^+ values are not usually available because steric effects often influence reactivity in this position. In the present case, however, there should

From linear regression of the Hammett plots in Fig. 5, values for ρ of -3.0 ± 0.3 and 2.9 ± 0.4 are obtained for decarboxylation of PAAs and Na-PAs, respectively. These are consistent with the formation of transient intermediates with opposite charges for the PAA and Na-PA reactions. In other words, the substituent effects demonstrate that associated acid molecules and acid anions decarboxylate via two different mechanisms.

4.2. Deducing mechanisms of decarboxylation

4.2.1. Phenylacetic acid

The positive charge that builds up in the benzene ring during hydrothermal decarboxylation of the phenylacetic acids can be explained if protonation of the benzene ring occurs, and if the rate of this protonation contributes to the overall rate of decarboxylation. On this basis, two possible mechanisms can be considered, indicated as **A** and **B** in the following reaction scheme

be protonated under hydrothermal conditions in the absence of strong acids (e.g., concentrated H_2SO_4), which are needed to drive protonation and form non-aromatic arenium ions at ambient conditions (Ingold, 1969; Olah et al., 1972; Cox, 1991). Nevertheless, reversible addition of protons/deuterons to benzene rings occurs when **PAA** is heated in deuterated water (D_2O). We previously conducted experiments in D_2O as the solvent with no other additives in which all five of the hydrogen atoms on the benzene ring in **PAA** were exchanged in as little as 23 h at 300 °C, presumably as a result of the combination of higher K_w (by a factor of $\sim$2400) and larger thermal energy compared with ambient (Glein, 2012).

Both mechanisms in reaction scheme (11) are consistent with the observed substituent effects (Fig. 5A), in addition to the moderate magnitude of the derived ρ value of -3 on the σ^+ scale. As an example, protonation at the *para*- or *ortho*-positions with respect to the acetic group can explain why a methyl substituent in the *meta*-position, *m*-

$$(11)$$

In scheme (11A), the PAA is reversibly protonated on the benzene ring to form a cationic intermediate, **C**. The rate constants for protonation and deprotonation are given by $k_1^A[H^+]$ and k_{-1}^A, respectively (11**A**), where the superscript A refers to the acid. *Para*-protonation is shown in scheme (11A) for the purpose of illustration, but *ortho*- protonation may also occur. **C** then undergoes loss of a proton to water, and *also* decarboxylation to form carbon dioxide and isotoluene (**iTol**), an isomer of the final product toluene (Bartmess, 1982), with rate constant k_2^A. Isotoluene is readily converted to the more stable aromatic toluene (**Tol**) via additional protonation and deprotonation steps. In the alternative mechanism, reaction scheme (11B), PAA first deprotonates to form the conjugate base carboxylate anion, **PAA⁻**, which is then reversibly ring-protonated to form a zwitterionic intermediate, **Z** (the rate constants involving the carboxylate anion are given a superscripted $-$). The zwitterion subsequently undergoes unimolecular decarboxylation to form the same isotoluene as in scheme (11A), which then forms the more stable final product toluene.

Reversible protonation of the benzene ring is required for both mechanisms, which is consistent with previous reports that ring protonation can activate other aromatic acids towards decarboxylation (Taylor 1972b; Willi, 1977). It may seem remarkable that the benzene ring can

Me-PAA in Table 5, gives the fastest rate of decarboxylation among the PAAs. According to scheme (8), a methyl group in the position *meta*- to the acetic group will donate electron density directly to the positively charged carbon to which it is bonded, which would stabilize the intermediate and thus increase the rate of decarboxylation (e.g., Hammond, 1955). Other reactions in which a positively charged species (e.g., D^+, NO_2^+) is added to the benzene ring (i.e., electrophilic aromatic substitution) also have negative ρ values on the σ^+ scale. Hydrogen isotope exchange in H_2O-H_2SO_4 at 100 °C has a ρ of -7.5 (Clementi and Katritzky, 1973). The decarboxylation of 4-substituted salicylic acids in water at 50 °C has a ρ of -4.4 (Willi, 1959). Nitration in nitromethane or acetic anhydride at ambient temperature has a ρ near -6, while chlorination and bromination in acetic acid at 25 °C have even more negative ρ values of approximately -8 and -12, respectively (Brown and Okamoto, 1958).
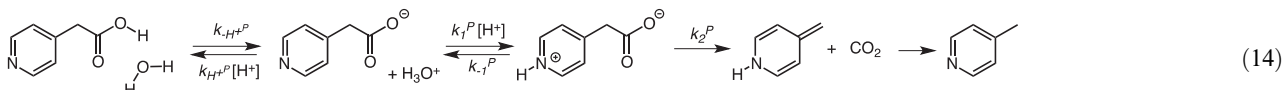
First-order kinetics are predicted by both mechanisms in scheme (11), consistent with the experimental data (Figs. 2–4). Application of the steady-state approximation for the intermediates leads to the rate equation

$$\frac{d[\textbf{PAA}]}{dt} = -\frac{k_1^A[H^+]\,k_2^A}{k_{-1}^A + k_2^A}[\textbf{PAA}] = -k_{app}[\textbf{PAA}]$$

$$(12)$$

for reaction scheme (11A), and

$$\frac{d[\mathbf{PAA}]}{dt} = -\frac{(k_{-H^+}/k_{H^+})\,k_1^-\,k_2^-}{k_{-1}^- + k_2^-}[\mathbf{PAA}] = -k_{app}[\mathbf{PAA}]$$

(13)

for reaction scheme (11B). In both cases, it is assumed that rearrangement of isotoluene to toluene is not rate-determining, based on observations that alkene rearrangement via protonation/deprotonation occurs on timescales that are much shorter than that for **PAA** decarboxylation (Bockisch et al., 2018). As indicated in Eqs. (12) and (13), there is no single rate-determining step for either mechanism, and the apparent rate constant for both mechanisms (where $k_{decarb} \approx k_{app}$, see Section 3.2; Table 5) is a composite of elementary rate constants. Importantly, k_{app} is directly proportional to k_1^A (11A) or k_1^- (11B), i.e., to the rate constant for formation of the positively charged benzene ring, consistent with the substituent effects discussed above. However, other elementary steps contribute to the

anism. Experiments were previously performed with **PAA** in the presence of 1 m HCl. Under these conditions, the reaction rate increased by a factor of only $\sim$1.6 relative to water alone, despite an estimated 560-fold increase in the concentration of H$^+$, which supports the (11B) mechanism. The small rate enhancement with 1 m HCl might be due to a change in ionic strength from 0.001 to 0.6 m (Glein, 2012). This dependence suggests that ionic strength has a minor effect on the reaction rate. However, this could be tested to assess activity effects on the stability of the zwitterion, by performing experiments in NaCl solution to modify the ionic strength without perturbing the pH.

These observations are consistent with the proposed mechanisms of decarboxylation of other arylacetic acids. Pyridylacetic acids are nitrogen heterocycle analogues of phenylacetic acids, and the proposed mechanism for their decarboxylation involves ring protonation of the corresponding carboxylates to form a zwitterion intermediate (Stermitz and Huang, 1971; Taylor, 1972a; Button and Taylor, 1973), shown schematically as
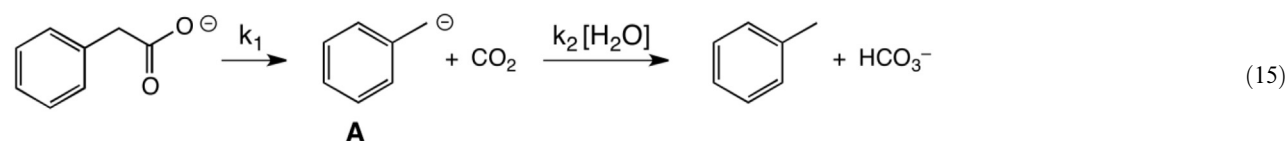

(14)

substituent effects, specifically the two decarboxylation steps, k_2^A and k_2^-. In each decarboxylation, the positive charge is removed from the benzene ring. Just as electron-donating groups increase the rate of protonation of the benzene ring by stabilizing the positive charge, electron-donating groups could slow decarboxylation for the same reason. In this way, the substituent effects may be diluted, which could account for the somewhat smaller value of ρ compared to other reactions that generate a positive charge on a benzene ring reviewed above.

The two schemes differ in the exact order of the various protonation and deprotonation steps. Distinguishing mechanisms involving similar ionic species in rapid equilibrium using kinetic data can be challenging (Frost and Pearson, 1961); nevertheless, evidence from this work and the literature favors the mechanism of reaction scheme (11B) over that of (11A). The mechanism of scheme (11B) may seem unlikely, given that the equilibrium concentration of **PAA**$^-$ is likely to be low. Furthermore, we show in Section 4.2.2 that in Na-PA solutions **PAA**$^-$ undergoes decarboxylation on its own, without protonation, to yield carbon dioxide and toluene via a different mechanism. Nevertheless, it should be noted that the (11B) mechanism differs from (11A) in that the apparent rate constant for reaction, k_{app}, does not depend upon the proton concentration, since [H$^+$] appears in both the rate of formation of the zwitterion (k_1^-[H$^+$]) and in the rate of protonation of **PAA**$^-$ (k_H^+[H$^+$]), and these cancel in the rate equation. In contrast, the apparent rate constant for reaction scheme (11A) depends directly on proton concentration. This implies a strong dependence of the rate on pH for the (11A) reaction mechanism, and no dependence on pH for the (11B) mech-

Reaction scheme (14) is analogous to (11B), with a pyridine ring in place of a benzene ring and where the superscript P on the rate constants indicates a pyridyl acid. The pyridylacetic acids decarboxylate much more rapidly than the **PAAs**, presumably a consequence of differences in the relative ease of protonation of the two aromatic rings. Aromatic nitrogen is orders of magnitude more basic than aromatic carbon, as demonstrated by the ambient pK_a's of their conjugate acids (e.g., ca. 5 for the pyridinium ion vs. ca. −24 for the benzenium ion; Lawlor et al., 2008). Support for the mechanism of scheme (14) for the pyridylacetic acids comes from several observations, at least two of which are relevant to **PAA**. First, decarboxylation when the pyridyl nitrogen is in the 2- or 4-position with respect to the acetic acid is much faster than the corresponding reaction when the nitrogen is in the 3-position. This is because the corresponding isomethylpyridine structure cannot form with the nitrogen in the 3-position, which provides support for the isomethylpyridine as an intermediate in the reaction, and by analogy, isotoluene in the **PAA** reaction. More importantly, decreasing the solution pH from 6.4 to 2.3 for both the 2- and 4-pyridyl acids increased the rate of reaction by a factor of only 3 and 4, respectively. This was taken as strong evidence in favor of protonation of the carboxylate to form the zwitterion intermediate, and by analogy, suggests protonation of the carboxylate anion for **PAA**.

If the **PAA** reaction proceeds via protonation of the carboxylate via reaction scheme (11B) and not via the associated acid in scheme (11A), then this imposes several kinetic constraints. First, decarboxylation in both the zwitterion **Z** (k_2^-) and the corresponding cation **C** (k_2^A) must

compete with deprotonation of the protonated benzene ring, k_{-1}^- and k_{-1}^A in **Z** and **C**, respectively. Protonated benzene rings are strong Brønsted acids, with pK_a values around −24 (Lawlor et al., 2008). Second, decarboxylation of the zwitterion **Z** must be much more competitive with deprotonation than the corresponding decarboxylation in **C**; otherwise, reaction would all occur from the acid (scheme 11A), and protonation of **PAA**$^-$ would not be necessary. It should be noted that decarboxylation of **Z** is unimolecular whereas deprotonation in **C** requires simultaneous, or close to simultaneous, deprotonation to avoid having to eliminate protonated carbon dioxide (Cummings et al., 2016), and is thus bimolecular. The protonated benzene ring in **C** is more acidic than the carboxylic acid by roughly 28 pK_a units; therefore, it may not be surprising that decarboxylation of **C** is not competitive with deprotonation. Unimolecular decarboxylation of **Z** does not require deprotonation, and unimolecular decarboxylation of zwitterionic radical cations of acetic acid carboxylates occurs on timescales as short as nanoseconds even at ambient conditions (Gould et al., 2004). Therefore, decarboxylation of **Z** may be expected to be much more competitive than in **C**. Third, reaction scheme (11B) also requires that protonation of **PAA**$^-$ and subsequent decarboxylation must be competitive with decarboxylation of **PAA**$^-$ itself, which as we show below, occurs via a different mechanism. However, that reaction is taking place in the presence of $1\,m$ **PAA** and together with the increased concentration of protons under hydrothermal conditions mentioned above, is sufficient to ensure that the majority of the **PAA**$^-$ reacts by protonation of the benzene ring first.

4.2.2. Sodium phenylacetate

The positive value of ρ for the decarboxylation of sodium phenylacetates (Fig. 5B) indicates that negative charge increases in the benzene ring during the reaction. This can be explained if a benzyl anion is the key intermediate. Based on this inference and other arguments discussed below, we propose an ionic, sequential mechanism for the decarboxylation of Na-PAs consistent with

bond heterolysis in the carboxylate, although the correspondence may not be exact because of the formation of aqueous complexes such as Na(PA) and Na(PA)$_2^-$ (Glein, 2012). Second, the proposed mechanism is consistent with the observation of a linear correlation with respect to σ^- as well as the associated ρ value (Fig. 5B), because the formation of the benzyl anion introduces negative charge into the aromatic system by resonance as in

$$\tag{17}$$
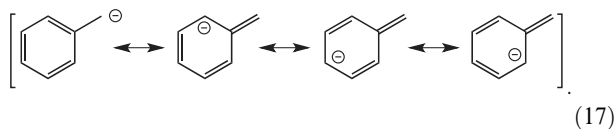
The presence of a negative charge on the *para* carbon in the benzyl anion can explain why the *p*-Me substituted carboxylate has the smallest rate constant for decarboxylation among the Na-PAs (Table 5), since donation of electrons from the methyl group to the *para* carbon leads to electron-electron repulsion that destabilizes the benzyl anion, raising the activation energy for its formation.

The ρ value (2.9) for the decarboxylation of Na-PAs (Fig. 5B) is similar to literature values derived from rates of reactions that also proceed via a benzyl anion. Streitwieser and Koch (1964) reported a ρ of 4.0 for cyclohexylamide-catalyzed hydrogen isotope exchange of toluenes in cyclohexylamine at 50 °C. Retroaldolization of 1-phenyl-2-arylcyclopropanol anions in H$_2$O-CH$_3$CN at 25 °C has a ρ of 4–5 (Thibblin and Jencks, 1979). The most direct comparison may be the decarboxylation of α-cyanophenylacetates that have the strong electron-withdrawing CN group on the benzylic (α) carbon. Straub and Bender (1972) determined a ρ of 2.44 for the decarboxylation of α-cyanophenylacetates in water at 60.4 °C. The similarity in ρ values suggests that phenylacetate and α-cyanophenylacetate decarboxylate via the same type of mechanism. However, α-cyanophenylacetate decarboxylates at much lower temperatures than phenylacetate because the cyano group is highly effective at stabilizing carbanions and the transition states through which they


$$\tag{15}$$

where the free carboxylate ion decarboxylates to the benzyl anion (**A**) as the rate-determining step. The benzyl anion, which is protonated by a water molecule to produce toluene, is assumed to be a transient intermediate.

This mechanism is consistent with several observations. First, it predicts first-order kinetics, consistent with the experimental data (Figs. 2–4) and

$$\frac{d[PAA^-]}{dt} = -k_1[PAA^-]. \tag{16}$$

Unlike the PAAs, the derived rate constants for the Na-PAs (Table 5) approximate the elementary rate constant for C-C

are formed (Hammond, 1955), as evidenced by the much greater acidity of acetonitrile (CH$_3$CN, $pK_a \approx 29$) vs. methane (CH$_3$H, $pK_a \approx 49$; Richard et al., 1999).

In further support of the proposed mechanism, decarboxylation via carbanion intermediates is one of the most well-established mechanisms in conventional organic chemistry (Brown, 1951; Smith and March, 2007). The reaction represents a type of electrophilic substitution where H$^+$ substitutes for CO$_2$ (Segura et al., 1985). Examples of this reaction mechanism include the decarboxylation of acids with strong electron-withdrawing groups attached to the carbon atom that is adjacent to the carboxyl carbon, such

as nitroacetic (NO₂CH₂COOH) and trihalogenic (*e.g.*, Cl₃-CCOOH, F₃CCOOH) acids. As in the previous case of α-cyanophenylacetate, these compounds decarboxylate readily at low temperatures because the electron-withdrawing group greatly stabilizes the carbanion intermediate.

While the high reactivity of carbanions (*e.g.*, Bockrath and Dorfman, 1974) makes them difficult to observe during decarboxylation, there is some direct evidence for their intermediacy in decarboxylation reactions. Atkins et al. (1984) showed that the trichloromethyl anion is produced from the decarboxylation of trichloroacetate, by trapping with 1,3,5-trinitrobenzene (TNB) in dimethyl sulfoxide at 25 °C, via

$$(18)$$
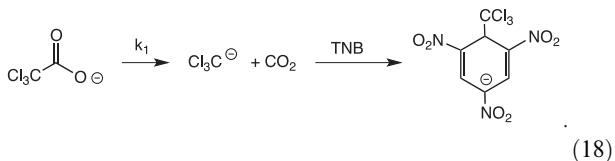
In addition, Buncel et al. (1984) detected benzyl anions by ultraviolet–visible spectrophotometry during the decarboxylation of ring-substituted nitrophenylacetates in polar aprotic solvents at room temperature.

The structures with substituents in the *ortho*-position have rate constants for decarboxylation that lie above the Hammett correlation line in Fig. 5B. Specific effects at the *ortho*-position are observed in many organic reactions, and they reflect a combination of inductive, resonance, and steric effects (Gould, 1959). Na-*o*-Me-PA decarboxylates faster than Na-PA (Table 5), but electron donation by this substituent should destabilize the benzyl anion, which should decrease the rate constant for decarboxylation relative to the parent compound. A steric effect could account for the unexpectedly high reactivity of Na-*o*-Me-PA if it is hypothesized that electron repulsion between the adjacent CH₃ and CH₂COO⁻ groups increases the energy of the reactant, while such a steric effect may be diminished as the carboxyl separates from the *o*-methylbenzyl group in the transition state for bond cleavage. Accordingly, the energy of the reactant is raised for Na-*o*-Me-PA, and thus the energy barrier to the transition state is decreased. In contrast, the *ortho* effect for Na-*o*-F-PA is less likely to be due to a steric effect, since F is smaller than CH₃ (Bondi, 1964). Nevertheless, Na-*o*-F-PA decarboxylates ~14 times faster than predicted (Fig. 5B). In this case, the explanation may simply be that the σ_p^- parameter is not accurate for fluorine substituents in this position. σ_p^- is calibrated primarily to account for inductive effects in the *para*-position, but a fluorine in the *ortho*-position could have a much larger inductive effect because it is significantly closer to the benzylic carbon. Evidently, the rate-enhancing inductive effect dominates any rate-retarding resonance effect for Na-*o*-F-PA, consistent with previous work where it was found that an *ortho*-fluorine enhances the rate of benzyl anion formation by deprotonation of toluenes (Streitwieser and Koch, 1964).

With these considerations in mind, we conclude that, in contrast to the decarboxylation mechanism of the associated acids, decarboxylation of the carboxylate anions of the phenylacetic acids occurs by heterolytic bond cleavage to form a carbon anion (carbanion) intermediate. These differences have implications for geochemical decarboxylation in general.

5. GEOCHEMICAL IMPLICATIONS

It is argued that hydrocarbons produced by decarboxylation could contribute to petroleum or natural gas accumulations (Cooper and Bray, 1963; Shimoyama and Johns, 1971; Carothers and Kharaka, 1978; Tissot and Welte, 1984; Ong et al., 2013). It follows that decarboxylation of carboxylic acids has been studied extensively (Brown, 1951; Clark, 1969; Richardson and O'Neal, 1972; Siskin and Katritzky, 1991; Bell and Palmer, 1994; Smith and March, 2007), including in high-temperature water, which is the solvent for many geochemical processes. The products and/or rates of decarboxylation in high-temperature water are reported for formic acid (Maiella and Brill, 1998; McCollom and Seewald, 2003a; Yasaka et al., 2006; Ong et al., 2013), oxalic acid (Crossey, 1991), acetic acid (Kharaka et al., 1983; Palmer and Drummond, 1986; Bell et al., 1994; McCollom and Seewald, 2003b; Ong et al., 2013; Li et al., 2017), acetic acid derivatives with electron-withdrawing groups (Belsky et al., 1999), malonic acid (Maiella and Brill, 1996), butyric acid (Palmer and Drummond, 1986), valeric acid (McCollom and Seewald, 2003b), palmitic acid (Fu et al., 2010), stearic acid (Watanabe et al., 2006), benzoic acid (Katritzky et al., 1990a, Fecteau et al., 2019), OH-substituted benzoic acids (Li and Brill, 2003), phenylacetic acid (Katritzky et al., 1990b), mandelic acid (Katritzky et al., 1990c), and citric acid (Cody et al., 2001). Although qualitative and quantitative observations related to decarboxylation under geochemically relevant conditions are presented in these studies, mechanisms of the reaction under such conditions are unclear (Bell and Palmer, 1994). Mechanistic explanations for decarboxylation reactions would allow experimental rate data to be generalized and extrapolated over the wide range of compounds and conditions characteristic of geological environments and would improve quantitative assessments of the involvement of carboxylic acids in geochemical processes. It follows that the mechanisms of decarboxylation of phenylacetic acid and its carboxylate can help explain the general phenomenon of decarboxylation in natural systems.

Because the associated phenylacetic acids and the phenylacetate anions decarboxylate via different mechanisms, we now know that the speciation of a carboxylic acid can determine the reaction mechanism and ensuing reaction rates. These differences highlight the importance of geochemical conditions such as pH in determining the reaction mechanism, and therefore reaction kinetics. The proposed mechanisms underscore the importance of possessing a structural feature close to the carboxyl group that can accept an electron pair to facilitate decarboxylation. In the case of phenylacetic acid, a protonated benzene ring in the zwitterion form of the acid serves as an electron sink, while for the carboxylate the electron sink is the delocalized benzyl group. As discussed below, these generalizations about speciation-dependent mechanisms and the key

requirement of an electron sink may translate to other carboxylic acids of equal or greater geochemical relevance.

Mechanistic differences involved in hydrothermal decarboxylation of associated acid molecules vs. their corresponding acid anions implies that decarboxylation rates may depend on pH. As indicated by the rate constants in Table 5, the acid anions tend to decarboxylate somewhat faster than the associated molecules at our experimental conditions. McCollom and Seewald (2003b) reported similar behavior for acetate and acetic acid decarboxylation rates in experiments in the presence of hematite and magnetite, or hematite, magnetite, and pyrite, but the rates were much closer to each other in experiments with pyrite, pyrrhotite, and magnetite. In contrast, acetic acid was found to react faster than acetate in mineral-free experiments conducted by Kharaka et al. (1983, Drummond and Palmer (1986), and Bell et al. (1994), although the distinction between decarboxylation, oxidation, and other reactions is unclear in many of these experiments (see McCollom and Seewald, 2003b). Additionally, McCollom and Seewald (2003a) reported that decarboxylation of formate is slower than that of formic acid, similar to results reported by Maiella and Brill (1998).

Keeping in mind the differences summarized above, generalizing from the pH dependence of decarboxylation in hydrothermal experiments reported here suggests that many carboxylic acids may persist somewhat longer at lower pH than at higher pH. The plot in Fig. 6 shows pK_a values of four representative carboxylic acids, together with a curve showing where neutral pH occurs, curves showing representative examples of situations where pH is governed by reactions between aqueous solutions and mineral assemblages in geochemical processes, and fields showing where oil-field brines and submarine hydrothermal fluids fall. The speciation of each carboxylic acid is dominated by the associated form at pH values less than its pK_a, and by the acid anion at pH values greater than its pK_a. Note that neutral pH falls on the side of anion predominance for acetic and propanoic acids at temperatures below about 200 °C, and for benzoic and o-toluic acids below about 300 °C. The curve in Fig. 6 labeled 'granitic alteration' corresponds to values of pH set by equilibrium between a 1 molal KCl solution and the mineral assemblage K-feldspar-muscovite-quartz, and that labeled 'serpentinization' corresponds to values set by equilibrium between a 1 molal $CaCl_2$ solution and a diopside-chrysotile-brucite assemblage (Robinson et al., 2019). Note that pH values for the granitic alteration example would favor the associated forms of carboxylic acids, especially at higher temperatures, and those for the serpentinization example would favor the anions. It can be expected that decarboxylation mechanisms will be distinctly different between these two geochemical environments. In sedimentary basins, where oil-field brines in the 50–150 °C range can be enriched in organic acids, pH values are thought to range from 1 to 2 pH units below neutrality (MacPherson, 1992) to 0.5 pH unit above (Helgeson et al., 1993) depending on the composition of minerals and fluids in individual geologic units. Results from the latter study fall within the oval on the left side of Fig. 6.
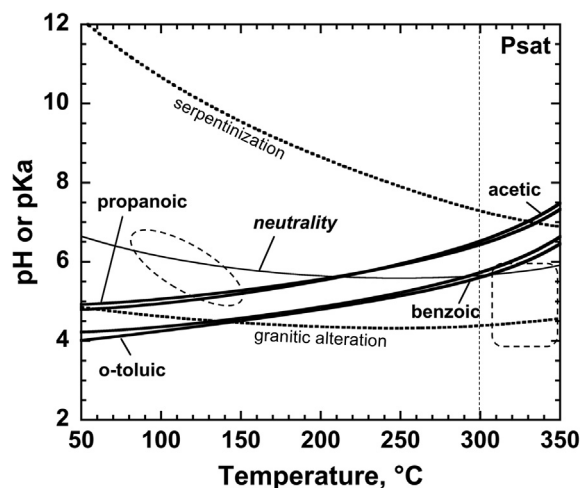

Fig. 6. pH-Temperature plot showing pK_a values for acetic, propanoic, benzoic, and o-toluic acids, calculated with the revised HKF equation of state using data and parameters reported by Shock (1995), together with curves depicting neutral pH and pH values calculated for mineral assemblages and fluids representative of granite- and serpentinite-hosted hydrothermal fluids (see text) at the saturation pressure of water. Phenylacetic acid is not shown because Gibbs free energy data for aqueous phenylacetic acid and phenylacetate are unavailable at high temperatures and pressures. However, based on pK_a relationships that include phenylacetic acid at 25 °C and 1 bar (compiled by R. Williams at https://www.chem.wisc.edu/areas/organic/index-chem.htm) and the relative positions of the pK_a curves in this figure, we estimate that the pK_a of phenylacetic acid should be similar to that of benzoic acid to within ~0.3 units. Note that associated forms of the acids would be dominant in mildly acidic granite-hosted fluids, but anionic forms would dominate in more basic serpentinite-hosted fluids. Also shown in the figure are general regions of pH and temperature for oil-field brines (lower temperature oval) and submarine hydrothermal fluids hosted in basalt (higher temperature box). For comparison, the experimental temperature in this study is indicated by the vertical dashed line. Different reaction mechanisms of the associated and anionic forms of aqueous organic acids, together with variations in pH driven by rock compositions in hydrothermal systems, imply that rates of hydrothermal organic acid decarboxylation will depend on the major-element composition of host rocks.

Examination of Fig. 6 suggests that there may be consequences of these pH differences for the persistence of organic acids relative to decarboxylation that could help explain the wide-ranging differences in organic acid concentrations among sedimentary basin brines even at the same temperature (Shock, 1994). Submarine hydrothermal fluids hosted in basalt typically fall close to the box on the right side of Fig. 6 (Shock and Canovas, 2010; German and Seyfried, 2014), indicating that the associated forms of the acids may dominate the mechanisms of decarboxylation in these systems.

The phenylacetic acid mechanism (scheme 11B) may be directly applicable to aromatic acids with an alpha-carboxyl, such as benzoic acid, which is found in oil-field brines (Barth, 1987; Fisher and Boles, 1990; Kawamura and Nissenbaum, 1992) and other natural waters (Khasanov et al., 2016). These aromatic systems can be activated to decarboxylation analogously to phenylacetic

acid by the formation of a reactive ring-protonated zwitterion. As an example, benzoic acid may decarboxylate via
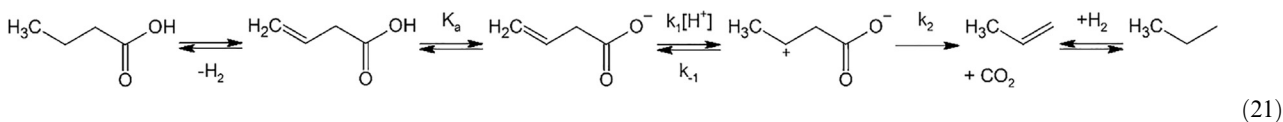

$$(19)$$
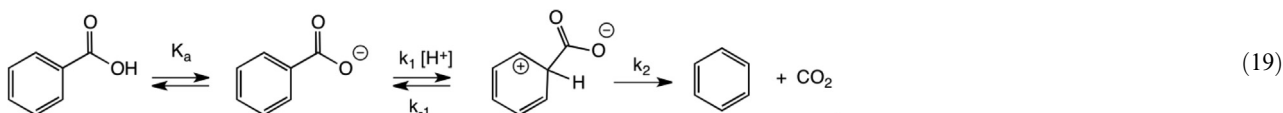
Because the carboxyl group is directly attached to the aromatic ring, the *ipso* carbon (rather than *para* or *ortho*) must be protonated to form a zwitterion that can serve as an electron sink for decarboxylation. In this case, the *ipso*-protonated zwitterion can form the final product benzene directly by decarboxylation, in contrast to the isotoluene rearrangement that is required for phenylacetic acid. The phenylacetic acid mechanism (scheme 11B) may also be directly applicable to more structurally complex compounds, such as polyaromatic acids, if there is a carboxyl that is in a *beta* position relative to one of the aromatic carbons. Any polycyclic aromatic carboxylic acid with unsaturation *alpha*- or *beta*- to the acid functional group can in principle decarboxylate the same way. For acids with a more displaced aromatic system (*e.g.*, phenylpropanoic acid), ring protonation creates an electron sink that is too far to accept electrons flowing from the carboxyl during decarboxylation. Such species should decarboxylate slowly, similar to aliphatic acids as described below.

A zwitterion activation process could also apply to the decarboxylation of alkanoic acids with three or more carbon-chain atoms. Under hydrothermal conditions, alkanes can be reversibly converted to alkenes (Seewald, 1994; Yang et al., 2012; Shipp et al., 2013). This suggests interconversion between alkanoic and alkenoic acids. Once a double bond is introduced, a zwitterion can be formed. Based on the benzoic acid mechanism (scheme 19) propanoic acid could decarboxylate via
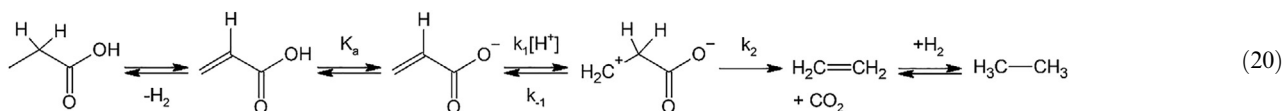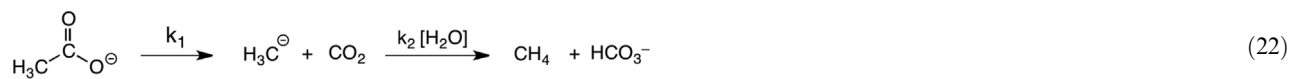
which is similar to that in the proposed mechanism for phenylacetic acid. If so, decarboxylation may occur faster in more oxidized geological environments that facilitate the formation of alkenoic acid intermediates.

A Brønsted plot of logarithmic rate constants for decarboxylation of several carboxylate anions vs. the pK_a of the corresponding decarboxylation products, shown in Fig. 7, is proposed as a step toward the development of a general quantitative model that accounts for different rates among decarboxylation reactions. The plot in Fig. 7 was made with rate constants from Belsky et al. (1999), Palmer and Drummond (1986), Bell et al. (1994), and this work, together with carbon-centered acidities from Lin et al. (1983), Streitwieser and Ni (1985), and Richard et al. (1999). If the decarboxylation reactions all occur via the type of mechanism as shown in scheme (15), then decarboxylation and deprotonation of the hydrocarbon product both generate the same carbanion intermediate and can in principle be quantitatively related. The linearity of the plot in Fig. 7 confirms this initial quantitative relationship.

As in the case of the Hammett plots in Fig. 5, the Brønsted plot in Fig. 7 implies a linear free energy relationship, which suggests that these species decarboxylate by the same type of carbanion mechanism as phenylacetate (scheme 15). If so, this helps clarify the decarboxylation mechanism of acetate, which is difficult to study directly because the acetate reaction is slow and lacks electron-withdrawing groups that would support a carbanion mechanism. We propose the following mechanism for acetate

$$(20)$$

where protonation is assumed to occur at the *alpha* carbon. In addition, decarboxylation of carboxylic acids with four or more chain carbons may include a competitive *gamma* protonation such as

$$(21)$$

$$\underset{\text{H}_3\text{C}}{\overset{\overset{\displaystyle O}{\|}}{\text{C}}}\underset{\text{O}^{\ominus}}{}\ \xrightarrow{k_1}\ \text{H}_3\text{C}^{\ominus}\ +\ \text{CO}_2\ \xrightarrow{k_2\,[\text{H}_2\text{O}]}\ \text{CH}_4\ +\ \text{HCO}_3^-$$

$$(22)$$

,

where the intermediate is the methide anion, H_3C^-. The slope (β) of the Brønsted plot is -0.4, which suggests that the transition state of the decarboxylation reaction has a moderate degree of carbanion character, and that the bond to the carboxyl carbon is almost halfway broken at the transition state. This β value is somewhat less negative than that (-0.7) derived by Wolfenden et al. (2011) at 25 °C, which could be explained by diminished selectivity at higher temperatures.

The Brønsted correlation can also be used as the basis of a predictive scheme for carboxylates that have not been studied experimentally. For example, the pK_a of ethane has been estimated to be ~ 52 (Jorgensen and Briggs, 1989), or ~ 3 orders of magnitude less acidic than methane. This suggests that propanoate should decarboxylate more slowly than acetate. Using Fig. 7, we predict that propanoate would decarboxylate ~ 1 order of magnitude slower than acetate, with a rate constant of $\sim 3 \times 10^{-10}$ s^{-1} at 300 °C. Longer-chain carboxylates would also decarboxylate to form primary (1°) carbanions and thus may decarboxylate with rate constants similar to that for propanoate at high temperature and pressure. This suggests that the dominance of acetate relative to longer-chain carboxylates in oil-field brines (Willey et al., 1975; Carothers and Kharaka, 1978; Fisher, 1987; Barth, 1991; Helgeson et al., 1993; Lundegard & Kharaka, 1994) may not be explained by the relative kinetics of decarboxylation of the alkanoic acids in hydrothermal solutions, since acetate would decarboxylate an order of magnitude faster than the other carboxylates. Instead, the high concentration of acetate may be explained by a faster rate of formation of acetate, compared to other carboxylates, or a difference in the way that decarboxylation is controlled in natural systems, for example by mineral catalysis, or both of the above. The Brønsted correlation brings us closer to the development of predictive decarboxylation models for hydrothermal systems. The incorporation of activation energies and volumes of decarboxylation reactions into a unifying mechanistic framework could be attempted next to better constrain rates over structure-temperature-pressure space.

Fig. 7. Brønsted plot of the logarithm of the rate constant for decarboxylation of carboxylate anions, in water at 300 °C, versus the pK_a of the hydrocarbon conjugate acids of the carbanion products of decarboxylation, estimated at 25 °C and atmospheric pressure. The rate data for the substituted acetates is extrapolated to 300 °C from data of Belsky et al. (1999), for phenylacetate from this work, and for acetate from data of Palmer and Drummond (1986). The Brønsted plot is a linear free energy relationship if the Gibbs free energy for dissociation of the hydrocarbon acids to give the carbanions is directly proportional to the activation energy for formation of the same carbanions by decarboxylation of the carboxylates.

APPENDIX A. SUPPLEMENTARY MATERIAL

Supplementary data to this article can be found online at https://doi.org/10.1016/j.gca.2019.11.003.

REFERENCES

Amend J. P., Amend A. C. and Valenza M. (1998) Determination of volatile fatty acids in the hot springs of Vulcano, Aeolian Islands, Italy. *Org. Geochem.* **28**, 699–705.

Anslyn E. V. and Dougherty D. A. (2006) *Modern physical organic chemistry*. University Science Books, Sausalito, California.

Atkins P. J., Gold V. and Marsh R. (1984) The decarboxylation of trichloroacetic acid and the reactions of the trichloromethyl anion with 1,3,5-trinitrobenzene and with hydrogen ions:
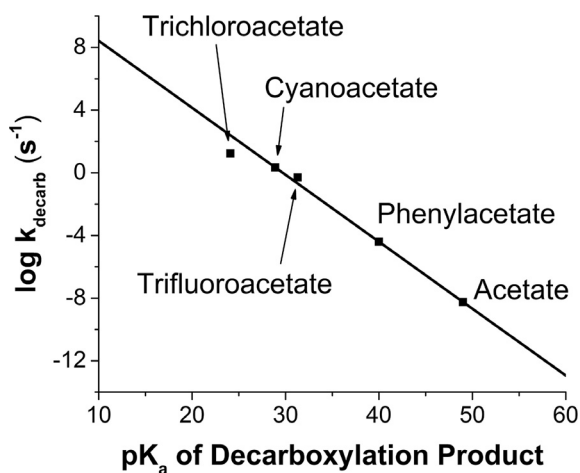
Kinetic measurements in dimethyl sulphoxide solution. *J. Chem. Soc. Perk. Trans. II* **7**, 1239–1245.

Barth T. (1987) Quantitative determination of volatile carboxylic acids in formation waters by isotachophoresis. *Anal. Chem.* **59**, 2232–2237.

Barth T. (1991) Organic acids and inorganic ions in waters from petroleum reservoirs, Norwegian continental shelf: A multivariate statistical analysis and comparison with American reservoir formation waters. *Appl. Geochem.* **6**, 1–15.

Bartmess J. E. (1982) Gas-phase ion chemistry of 5-methylene-1,3-cyclohexadiene (*o*-isotoluene) and 3-methylene-1,4-cyclohexadiene (*p*-isotoluene). *J. Am. Chem. Soc.* **104**, 335–337.

Bell J. L. S. and Palmer D. A. (1994) Experimental studies of organic acid decomposition. In *Organic Acids in Geological Processes* (eds. E. D. Pittman and M. D. Lewan). Springer-Verlag, Berlin, pp. 226–269.

Bell J. L. S., Palmer D. A., Barnes H. L. and Drummond S. E. (1994) Thermal decomposition of acetate: III. Catalysis by mineral surfaces. *Geochim. Cosmochim. Acta* **58**, 4155–4177.

Beller H. R., Rodrigues A. V., Zargar K., Wu Y.-W., Saini A. K., Saville R. M., Pereira J. H., Adams P. D., Tringe S. G., Petzold C. J. and Keasling J. D. (2018) Discovery of enzymes for toluene synthesis from anoxic microbial communities. *Nat. Chem. Biol.* **14**, 451–457.

Belsky A. J., Maiella P. G. and Brill T. B. (1999) Spectroscopy of hydrothermal reactions. 13. Kinetics and mechanisms of decarboxylation of acetic acid derivatives at 100–260°C under 275 bar. *J. Phys. Chem. A* **103**, 4253–4260.

Bockisch C., Lorance E. D., Hartnett H. E., Shock E. L. and Gould I. R. (2018) Kinetics and mechanisms of dehydration of secondary alcohols under hydrothermal conditions. *ACS Earth Space Chem.* **2**, 821–832.

Bockrath B. and Dorfman L. M. (1974) Submicrosecond formation and observation of reactive carbanions. *J. Am. Chem. Soc.* **96**, 5708–5715.

Bondi A. (1964) van der Waals volumes and radii. *J. Phys. Chem.* **68**, 441–451.

Bradley J. A., Amend J. P. and LaRowe D. E. (2018) Bioenergetic controls on microbial ecophysiology in marine sediments. *Front. Microbiol.* **9**, 180. https://doi.org/10.3389/fmicb.2018.00180.

Breuker A., Köweker G., Blazejak A. and Schippers A. (2011) The deep biosphere in terrestrial sediments in the Chesapeake Bay area, Virginia, USA. *Front. Microbiol.* **2**, 156. https://doi.org/10.3389/fmicb.2011.00156.

Brown B. R. (1951) The mechanism of thermal decarboxylation. *Q. Rev. Chem. Soc.* **5**, 131–146.

Brown H. C. and Okamoto Y. (1958) Electrophilic substituent constants. *J. Am. Chem. Soc.* **80**, 4979–4987.

Buncel E., Venkatachalam T. K. and Menon B. C. (1984) A spectrophotometric study of 4-nitro-, 2,4-dinitro- and 2,4,6-trinitrobenzyl carbanions. Decarboxylation of (nitrophenyl) acetate anions. *J. Org. Chem.* **49**, 413–417.

Button R. G. and Taylor P. J. (1973) The decarboxylation of some heterocyclic acetic acids. Part II. Direct and indirect evidence for the zwitterionic mechanism. *J. Chem. Soc. Perk. Trans. II* **5**, 557–567.

Canovas, III, P. C. and Shock E. L. (2016) Geobiochemistry of metabolism: Standard state thermodynamic properties of the citric acid cycle. *Geochim. Cosmochim. Acta* **195**, 293–322.

Carothers W. W. and Kharaka Y. K. (1978) Aliphatic acid anions in oil-field waters – Implications for origin of natural gas. *AAPG Bull.* **62**, 2441–2453.

Clark L. W. (1969) The decarboxylation reaction. In *The Chemistry of Carboxylic Acids and Esters* (ed. S. Patai). Interscience-Publishers, Hungary, pp. 589–622.

Clementi S. and Katritzky A. R. (1973) The kinetics and mechanism of the electrophilic substitution of heteroaromatic compounds. Part XXXIII. Hammett treatment for hydrogen exchange of monosubstituted benzenes in sulphuric acid under standard conditions. *J. Chem. Soc. Perk. Trans. II* **7**, 1077–1080.

Cody G. D., Boctor N. Z., Hazen R. M., Brandes J. A., Morowitz H. J. and Yoder H. S. (2001) Geochemical roots of autotrophic carbon fixation: Hydrothermal experiments in the system citric acid, H_2O-(±FeS)-(±NiS). *Geochim. Cosmochim. Acta* **65**, 3557–3576.

Cooper J. E. and Bray E. E. (1963) A postulated role of fatty acids in petroleum formation. *Geochim. Cosmochim. Acta* **27**, 1113–1127.

Cox R. A. (1991) Isotope effects in acid-catalyzed aromatic hydrogen exchange. *J. Phys. Org. Chem.* **4**, 233–241.

Cozzarelli I. M., Herman J. S. and Baedecker M. J. (1995) Fate of microbial metabolites of hydrocarbons in a coastal plain aquifer: The role of electron acceptors. *Environ. Sci. Technol.* **29**, 458–469.

Crossey L. J. (1991) Thermal degradation of aqueous oxalate species. *Geochim. Cosmochim. Acta* **55**, 1515–1527.

Cummings S., Hratchian H. P. and Reed C. A. (2016) The strongest acid: Protonation of carbon dioxide. *Angew. Chem. Int. Edit.* **55**, 1382–1386.

Di Gioia D., Fava F. and Marchetti L. (2001) Biodegradation of hydroxylated and methoxylated benzoic, phenylacetic and phenylpropenoic acids present in olive mill wastewaters by two bacterial strains. *Res. Microbiol.* **152**, 83–93.

Drake H., Whitehouse M. J., Heim C., Reiners P. W., Tillberg M., Hogmalm K. J., Dopson M., Broman C. and Åström M. E. (2018) Unprecedented ^{34}S-enrichment of pyrite formed following microbial sulfate reduction in fractured crystalline rocks. *Geobiology* **16**, 556–574.

Drummond S. E. and Palmer D. A. (1986) Thermal decarboxylation of acetate. Part II. Boundary conditions for the role of acetate in the primary migration of natural gas and the transportation of metals in hydrothermal systems. *Geochim. Cosmochim. Acta* **50**, 825–833.

Fecteau K. M., Gould I. R., Glein C. R., Williams L. B., Hartnett H. E. and Shock E. L. (2019) Production of carboxylic acids from aldehydes under hydrothermal conditions: A kinetics study of benzaldehyde. *ACS Earth Space Chem.* **3**, 170–191.

Fisher J. B. (1987) Distribution and occurrence of aliphatic acid anions in deep subsurface waters. *Geochim. Cosmochim. Acta* **51**, 2459–2468.

Fisher J. B. and Boles J. R. (1990) Water-rock interaction in Tertiary sandstones, San Joaquin basin, California, U.S.A.: Diagenetic controls on water composition. *Chem. Geol.* **82**, 83–101.

Flores R. M., Rice C. A., Stricker G. D., Warden A. and Ellis M. S. (2008) Methanogenic pathways of coal-bed gas in the Powder River Basin, United States: The geologic factor. *Int. J. Coal Geol.* **76**, 52–75.

Fortunado C. S., Larson B., Butterfield D. A. and Huber J. A. (2018) Spatially distinct, temporally stable microbial populations mediate biogeochemical cycling at and below the seafloor in hydrothermal vent fluids. *Environ. Microbiol.* **20**, 769–784.

Franks S. G., Dias R. F., Freeman K. H., Boles J. R., Holba A., Fincannon A. L. and Jordan E. D. (2001) Carbon isotopic composition of organic acids in oil field waters, San Joaquin Basin, California, USA. *Geochim. Cosmochim. Acta* **65**, 1301–1310.

Fredrickson J. K. and Balkwill D. L. (2006) Geomicrobial processes and biodiversity in the deep terrestrial subsurface. *Geomicrobiol. J.* **23**, 345–356.

Frost A. A. and Pearson R. G. (1961) *Kinetics and Mechanism*. Wiley, New York, New York.

Fry J. C., Horsfield B., Sykes R., Cragg B. A., Heywood C., Kim G. T., Manglesdorf K., Mildenhall D. C., Rinna J., Vieth A., Zink K.-G., Sass H., Weightman A. J. and Parkes R. J. (2009) Prokaryotic populations and activities in an interbedded coal deposit, including a previously deeply buried section (1.6-2.3 km) above ~150 Ma basement rock. *Geomicrobiol. J.* **26**, 163–178.

Fu J., Lu X. and Savage P. E. (2010) Catalytic hydrothermal deoxygenation of palmitic acid. *Energ. Environ. Sci.* **3**, 311–317.

Fukuda A., Hagiwara H., Ishimura T., Kouduka M., Ioka S., Amano Y., Tsunogai U., Suzuki Y. and Mizuno T. (2010) Geomicrobiological properties of ultra-deep granitic groundwater from the Mizunami Underground Research Laboratory (MIU), Central Japan. *Microb. Ecol.* **60**, 214–225.

German C. R. and Seyfried, Jr., W. E. (2014) Hydrothermal Processes. In *Treatise on Geochemistry*. Elsevier, pp. 191–233. https://doi.org/10.1016/B978-0-08-095975-7.00607-0.

Glein C. R. (2012) *Theoretical and Experimental Studies of Cryogenic and Hydrothermal Organic Geochemistry* (Doctoral Dissertation). Arizona State University, Tempe, Arizona.

Glombitza C., Jaussi M., Røy H., Seidenkrantz M.-S., Lomstein B. A. and Jørgensen B. B. (2015) Formate, acetate, and propionate as substrates for sulfate reduction in sub-arctic sediments of Southwest Greenland. *Front. Microbiol.* **6**, 846. https://doi.org/10.3389/fmicb.2015.00846.

Gould E. S. (1959) *Mechanism and Structure in Organic Chemistry*. Holt, Rinehart and Winston, New York.

Gould I. R., Lenhard J. R. and Farid S. (2004) A curve-crossing model for oxidative decarboxylation. Kinetics of anilino carboxylate fragmentations. *J. Phys. Chem. A* **108**, 10949–10956.

Graw M. F., D'Angelo G., Borchers M., Thurber A. R., Johnson J. E., Zhang C., Liu H. and Colwell F. S. (2018) Energy gradients structure microbial communities across sediment horizons in deep marine sediments of the South China Sea. *Front. Microbiol.* **9**, 729. https://doi.org/10.3389/fmicb.2018.00729.

Hammett L. P. (1937) The effect of structure upon the reactions of organic compounds. Benzene derivatives. *J. Am. Chem. Soc.* **59**, 96–103.

Hammond G. S. (1955) A correlation of reaction rates. *J. Am. Chem. Soc.* **77**, 334–338.

Hansch C., Leo A. and Taft R. W. (1991) A survey of Hammett substituent constants and resonance and field parameters. *Chem. Rev.* **91**, 165–195.

Hawkes J. A., Rossel P. E., Stubbins A., Butterfield D., Connelly D. P., Achterberg E. P., Koschinsky A., Chavagnac V., Hansen C. T., Bach W. and Dittmar T. (2015) Efficient removal of recalcitrant deep-ocean dissolved organic matter during hydrothermal circulation. *Nat. Geosci.* **8**, 856–860.

Hawkes J. A., Hansen C. T., Goldhammer T., Bach W. and Dittmar T. (2016) Molecular alteration of marine dissolved organic matter under experimental hydrothermal conditions. *Geochim. Cosmochim. Acta* **175**, 68–85.

Helgeson H. C., Knox A. M., Owens C. E. and Shock E. L. (1993) Petroleum, oil field waters, and authigenic mineral assemblages: Are they in metastable equilibrium in hydrocarbon reservoirs?. *Geochim. Cosmochim. Acta* **57**, 3295–3339.

Heuer V. B., Pohlman J. W., Torres M. E., Elvert M. and Hinrichs K.-U. (2009) The stable carbon isotope biogeochemistry of acetate and other dissolved carbon species in deep subseafloor sediments at the northern Cascadia Margin. *Geochim. Cosmochim. Acta* **73**, 3323–3336.

Ingold C. K. (1969) *Structure and Mechanism in Organic Chemistry*, second ed. Cornell University Press, Ithaca, New York.

Ino K., Konno U., Kouduka M., Hirota A., Togo Y. S., Fukuda A., Komatsu D., Tsunogai U., Tanabe A. S., Yamamoto S., Iwatsuki T., Mizuno T., Ito K. and Suzuki Y. (2016) Deep microbial life in high-quality granitic groundwater from geochemically and geographically distinct underground boreholes. *Env. Microbiol. Rep.* **8**, 285–294.

Ino K., Hernsdorf A. W., Konno U., Kouduka M., Yanagawa K., Kato S., Sunamura M., Hirota A., Togo Y. S., Ito K., Fukuda A., Iwatsuki T., Mizuno T., Komatsu D. D., Tsunogai U., Ishimura T., Amano Y., Thomas B. C., Banfield J. J. and Suzuki Y. (2018) Ecological and genomic profiling of anaerobic methane-oxidizing archaea in a deep granitic environment. *ISME J.* **12**, 31–47.

Johnson C. D. (1973) *The Hammett Equation*. Cambridge University Press, London.

Jorgensen W. L. and Briggs J. M. (1989) A priori pKa calculations and the hydration of organic anions. *J. Am. Chem. Soc.* **111**, 4190–4197.

Katritzky A. R., Balasubramanian M. and Siskin M. (1990a) Aqueous high-temperature chemistry of carbo- and heterocycles. 2. Monosubstituted benzenes: Benzyl alcohol, benzaldehyde, and benzoic acid. *Energ. Fuel.* **4**, 499–505.

Katritzky A. R., Luxem F. J. and Siskin M. (1990b) Aqueous high-temperature chemistry of carbo- and heterocycles. 5. Monosubstituted benzenes with a two carbon atom side chain oxygenated at the β-position. *Energ. Fuel.* **4**, 514–517.

Katritzky A. R., Luxem F. J. and Siskin M. (1990c) Aqueous high-temperature chemistry of carbo- and heterocycles. 7. Monosubstituted benzenes with two carbon atom side chains oxygenated at the α- and β-positions. *Energ. Fuel.* **4**, 525–531.

Kawamura K. and Nissenbaum A. (1992) High abundance of low molecular weight organic acids in hypersaline spring water associated with a salt diapir. *Org. Geochem.* **18**, 469–476.

Kevorkian R., Bird J. T., Shumaker A. and Lloyd K. G. (2018) Estimating population turnover rates by relative quantification methods reveals microbial dynamics in marine sediment. *Appl. Environ. Microbiol.* **84**, e01443–e1517.

Kharaka Y. F., Carothers W. W. and Rosenbauer R. J. (1983) Thermal decarboxylation of acetic acid: Implications for origin of natural gas. *Geochim. Cosmochim. Acta* **47**, 397–402.

Khasanov V. V., Makarycheva A. I. and Slizhov Yu. G. (2016) Determination of aliphatic acids in natural waters using distillation and solid-phase extraction. *J. Anal. Chem.* **71**, 1028–1032.

Klein F., Humphris S. E., Guo W., Schubotz F., Schwarzanbach E. M. and Orsi W. D. (2015) Fluid mixing and the deep biosphere of a fossil Lost City-type hydrothermal system at the Iberia Margin. *Proc. Nat. Acad. Sci. USA* **112**, 12036–12041.

Konn C., Donval J. P., Guyader V., Roussel E., Fourré E., Jean-Baptiste P., Pelleter E., Charlou J. L. and Fouquet Y. (2018) Organic, Gas, and Element Geochemistry of Hydrothermal Fluids of the Newly Discovered Extensive Hydrothermal Area in the Wallis and Futuna Region (SW Pacific). *Geofluids* **2018**, 1–25. https://doi.org/10.1155/2018/7692839.

Konno U., Kouduka M., Komatsu D. D., Ishii K., Fukuda A., Tsunogai U., Ito K. and Suzuki Y. (2013) Novel microbial populations in deep granitic groundwater from Grimsel Test Site, Switzerland. *Microb. Ecol.* **65**, 626–637.

Lang S. Q., Butterfield D. A., Schulte M., Kelley D. S. and Lilley M. D. (2010) Elevated concentrations of formate, acetate and dissolved organic carbon found at the Lost City hydrothermal field. *Geochim. Cosmochim. Acta* **74**, 941–952.

Lang S. Q., Früh-Green G. L., Bernasconi S. M., Lilley M. D., Proskurowski G., Méhay S. and Butterfield D. A. (2012) Microbial growth on abiotic carbon and hydrogen in a

serpentinite-hosted system. *Geochim. Cosmochim. Acta* **92**, 82–99.

Lang S. Q., Früh-Green G. L., Bernasconi S. M. and Butterfield D. A. (2013) Sources of organic nitrogen at the serpentinite-hosted Lost City hydrothermal field. *Geobiology* **11**, 154–169.

Lang S. Q., Früh-Green G. L., Bernasconi S. M., Brazelton W. J., Schrenk M. O. and McGonigle J. M. (2018) Deeply-sourced formate fuels sulfate reducers but not methanogens at Lost City hydrothermal field. *Sci. Rep.* **8**, 755. https://doi.org/10.1038/s41598-017-19002-5.

LaRowe D. E., Burwicz E., Arndt S., Dale A. W. and Amend J. P. (2017) Temperature and volume of global marine sediments. *Geology* **45**, 275–278.

Lawlor D. A., More O'Ferrall R. A. and Rao S. N. (2008) Stabilities and partitioning of arenonium ions in aqueous media. *J. Am. Chem. Soc.* **130**, 17997–18007.

Li J. and Brill T. B. (2003) Spectroscopy of hydrothermal reactions 23: The effect of OH substitution on the rates and mechanisms of decarboxylation of benzoic acid. *J. Phys. Chem. A* **107**, 2667–2673.

Li Y., Zhou S., Li J., Ma Y., Chen K., Wu Y. and Zhang Y. (2017) Experimental study of the decomposition of acetic acid under conditions relevant to deep reservoirs. *Appl. Geochem.* **84**, 306–313.

Lin A. C., Chiang Y., Dahlberg D. B. and Kresge A. J. (1983) Base-catalyzed hydrogen exchange of phenylacetylene and chloroform. Brønsted relations and normal acid behavior. *J. Am. Chem. Soc.* **105**, 5380–5386.

Lin L. H., Wang P. L., Rumble D., Lippmann-Pipke J., Boice E., Pratt L. M., Sherwood Lollar B., Brodie E. L., Hazen T. C., Andersen G. L., DeSantis T. Z., Moser D. P., Kershaw D. and Onstott T. C. (2006) Long-term sustainability of a high-energy, low-diversity crustal biome. *Science* **314**, 479–482.

Lundegard P. D. and Kharaka Y. K. (1994) Distribution and occurrence of organic acids in subsurface waters. In *Organic Acids in Geological Processes* (eds. E. D. Pittman and M. D. Lewan). Springer-Verlag, Berlin, pp. 40–69.

MacGowan D. B. and Surdam R. C. (1990) Carboxylic acid anions in formation waters: San Joaquin Basin and Louisiana Gulf Coast, USA: Implications for clastic diagenesis. *Appl. Geochem.* **5**, 687–701.

MacPherson G. L. (1992) Regional variations in formation water chemistry: Major and minor elements, Frio formation fluids, Texas. *AAPG Bull.* **76**, 140–757.

Magnabosco C., Ryan K., Lau M. C. Y., Kuloyo O., Sherwood Lollar B., Kieft T. L., van Heerden E. and Onstott T. C. (2016) A metagenomic window into carbon metabolism at 3 km depth in Precambrian continental crust. *ISME J.* **10**, 730–741.

Maiella P. G. and Brill T. B. (1996) Spectroscopy of hydrothermal reactions. 5. Decarboxylation kinetics of malonic acid and monosodium malonate. *J. Phys. Chem.* **100**, 14352–14355.

Maiella P. G. and Brill T. B. (1998) Spectroscopy of hydrothermal reactions. 10. Evidence of wall effects in decarboxylation kinetics of 1.00 *m* HCO₂X (X = H, Na) at 280–330 °C and 275 bar. *J. Phys. Chem.* **102**, 5886–5891.

Manning C. E., Shock E. L. and Sverjensky D. A. (2013) The chemistry of carbon in aqueous fluids at crustal and upper-mantle conditions: Experimental and theoretical constraints. *Rev. Mineral. Geochem.* **75**, 109–148.

Martin W. F. (2016) Physiology, phylogeny, and the energetic roots of life. *Period. Biol.* **118**, 343–352.

McCollom T. M. and Seewald J. S. (2003a) Experimental constraints on the hydrothermal reactivity of organic acids and acid anions: I. Formic acid and formate. *Geochim. Cosmochim. Acta* **67**, 3625–3644.

McCollom T. M. and Seewald J. S. (2003b) Experimental study of the hydrothermal reactivity of organic acids and acid anions: II. Acetic acid, acetate, and valeric acid. *Geochim. Cosmochim. Acta* **67**, 3645–3664.

McCollom T. M., Seewald J. S. and Simoneit B. R. T. (2001) Reactivity of monocyclic aromatic compounds under hydrothermal conditions. *Geochim. Cosmochim. Acta* **65**, 455–468.

McDermott J. M., Seewald J. S., German C. R. and Sylva S. P. (2015) Pathways for abiotic organic synthesis at submarine hydrothermal fields. *Proc. Natl. Acad. Sci. USA* **112**, 7668–7672.

Means J. L. and Hubbard N. (1987) Short-chain aliphatic acid anions in deep subsurface brines: A review of their origin, occurrence, properties, and importance and new data on their distribution and geochemical implications in the Palo Duro Basin Texas. *Org. Geochem.* **11**, 177–191.

Moe W. M., Reynolds S. J., Griffin M. A. and McReynolds J. B. (2018) Bioremediation strategies aimed at stimulating chlorinated solvent dehalogenation can lead to microbially-mediated toluene biogenesis. *Environ. Sci. Technol.* **52**, 9311–9319.

Momper L., Reese B. K., Zinke L., Wanger G., Osburn M. R., Moser D. and Amend J. P. (2017) Major phylum-level differences between porefluid and hot rock bacterial communities in the terrestrial deep subsurface. *Env. Microbiol. Rep.* **9**, 501–511.

Morrison T. J. (1944) The salting-out effect. *Trans. Faraday Soc.* **40**, 43–48.

Neely B. J., Wagner J., Robinson, Jr., R. L. and Gasem K. A. M. (2008) Mutual solubility measurements of hydrocarbon-water systems containing benzene, toluene, and 3-methylpentane. *J. Chem. Eng. Data* **53**, 165–174.

Olah G. A., Schlosberg R. H., Porter R. D., Mo Y. K., Kelly D. P. and Mateescu G. D. (1972) Stable carbocations. CXXIV. The benzenium ion and monoalkylbenzenium ions. *J. Am. Chem. Soc.* **94**, 2034–2043.

Ong A., Pironon J., Robert P., Dubessy J., Caumon M.-C., Randi A., Chailan O. and Girard J.-P. (2013) In situ decarboxylation of acetic and formic acids in aqueous inclusions as a possible way to produce excess CH₄. *Geofluids* **13**, 298–304.

Onstott T. C., Moser D. P., Pfiffner S. M., Fredrickson J. K., Brockman F. J., Phelps T. J., White D. C., Peacock A., Balkwill D., Hoover R., Krumholz L. R., Borscik M., Kieft T. L. and Wilson R. (2003) Indigenous and contaminant microbes in ultradeep mines. *Environ. Microbiol.* **5**, 1168–1191.

Palmer D. A. and Drummond S. E. (1986) Thermal decarboxylation of acetate. Part I. The kinetics and mechanism of reaction in aqueous solution. *Geochim. Cosmochim. Acta* **50**, 813–823.

Parnell J. and McMahon S. (2016) Physical and chemical controls on habitats for life in the deep subsurface beneath continents and ice. *Phil. Trans. R. Soc. A* **374**, 20140293. https://doi.org/10.1098/rsta.2014.0293.

Parnell J., Baba M., Bowden S. and Muirhead D. (2017) Subsurface biodegradation of crude oil in a fractured basement reservoir, Shropshire, UK. *J. Geol. Soc.* **174**, 655–666.

Pedersen K. (1997) Microbial life in granitic rock. *FEMS Microbiol. Rev.* **20**, 399–414.

Pedersen K. and Ekendahl S. (1990) Distribution and activity of bacteria in deep granitic groundwaters of southeastern Sweden. *Microb. Ecol.* **20**, 37–52.

Pizzarello S. and Shock E. (2017) Carbonaceous chondrite meteorites: The chronicle of an evolutionary path between stars and life. *Origins Life Evol. B.* **47**, 249–260.

Plyasunov A. V. and Shock E. L. (2001) Correlation strategy for determining the parameters of the revised Helgeson-Kirkham-

Flowers model for aqueous nonelectrolytes. *Geochim. Cosmochim. Acta* **65**, 3879–3900.

Postberg F., Khawaja N., Abel B., Choblet G., Glein C. R., Gudipati M. S., Henderson B. L., Hsu H.-W., Kempf S., Klenner F., Moragas-Klostermeyer G., Magee B., Nölle L., Perry M., Reviol R., Schmidt J., Srama R., Stolz F., Tobie G., Trieloff M. and Waite J. H. (2018) Macromolecular organic compounds from the depths of Enceladus. *Nature* **558**, 564–568.

Price L. C. (1981) Aqueous solubility of crude oil to 400°C and 2,000 bars pressure in the presence of gas. *J. Petrol. Geol.* **4**, 195–223.

Reese B. K., Zinke L. A., Sobol M. S., LaRowe D. E., Orcutt B. N., Zhang X., Jaekel U., Wang F., Dittmar T., Defforey D., Tully B., Paytan A., Sylvan J. B., Amend J. P., Edwards K. J. and Girguis P. (2018) Nitrogen cycling of active bacteria within oligotrophic sediment of the mid-Atlantic ridge flank. *Geomicrobiol. J.* **35**, 468–483.

Richard J. P., Williams G. and Gao J. (1999) Experimental and computational determination of the effect of the cyano group on carbon acidity in water. *J. Am. Chem. Soc.* **121**, 715–726.

Richardson W. H. and O'Neal H. E. (1972) The unimolecular decomposition and isomerization of oxygenated organic compounds (other than aldehydes and ketones). In *Comprehensive Chemical Kinetics: Decomposition and Isomerisation of Organic Compounds* (eds. C. H. Bamford and C. F. H. Tipper). Elsevier Publishing Company, Amsterdam, pp. 381–565.

Riedinger N., Strasser M., Harris R. N., Klockgether G., Lyons T. W. and Screaton E. J. (2015) Deep subsurface carbon cycling in the Nankai Trough (Japan) – Evidence of tectonically induced stimulation of a deep microbial biosphere. *Geochem. Geophys. Geosys.* **16**, 3257–3270.

Robbins S. J., Evans P. N., Esterle J. S., Golding S. D. and Tyson G. W. (2016) The effect of coal rank on biogenic methane potential and microbial composition. *Int. J. Coal Geol.* **154–155**, 205–212.

Robinson K. J., Gould I. R., Fecteau K. M., Hartnett H. E., Williams L. B. and Shock E. L. (2019) Deamination reaction mechanisms of protonated amines under hydrothermal conditions. *Geochim. Cosmochim. Acta* **244**, 113–128.

Sahl J. W., Schmidt R. H., Swanner E. D., Mandernack K. W., Templeton A. S., Kieft T. L., Smith R. L., Sanford W. E., Callaghan R. L., Mitton J. B. and Spear J. R. (2008) Subsurface microbial diversity in deep-granitic-fracture water in Colorado. *Appl. Environ. Microbiol.* **74**, 143–152.

Schlegel M. E., McIntosh J. C., Bates B. L., Kirk M. F. and Martini A. M. (2011) Comparison of fluid geochemistry and microbiology of multiple organic-rich reservoirs in the Illinois Basin, USA: Evidence for controls on methanogenesis and microbial transport. *Geochim. Cosmochim. Acta* **75**, 1903–1919.

Schmitt R., Langguth H.-R., Püttmann W., Rohns H. P., Eckert P. and Schubert J. (1996) Biodegradation of aromatic hydrocarbons under anoxic conditions in a shallow sand and gravel aquifer of the Lower Rhine Valley, Germany. *Org. Geochem.* **25**, 41–50.

Schulte M. and Shock E. (2004) Coupled organic synthesis and mineral alteration on meteorite parent bodies. *Meteorit. Planet. Sci.* **39**, 1577–1590.

Seewald J. S. (1994) Evidence for metastable equilibrium between hydrocarbons under hydrothermal conditions. *Nature* **370**, 285–287.

Seewald J. S. (2001a) Aqueous geochemistry of low molecular weight hydrocarbons at elevated temperatures and pressures: Constraints from mineral buffered laboratory experiments. *Geochim. Cosmochim. Acta* **65**, 1641–1664.

Seewald J. S. (2001b) Model for the origin of carboxylic acids in basinal brines. *Geochim. Cosmochim. Acta* **65**, 3779–3789.

Seewald J. S. (2003) Organic-inorganic interactions in petroleum-producing sedimentary basins. *Nature* **426**, 327–333.

Segura P., Bunnett J. F. and Villanova L. (1985) Substituent effects on the decarboxylation of dinitrobenzoate ions. Representative aromatic S_E1 reactions. *J. Org. Chem.* **50**, 1041–1045.

Shimoyama A. and Johns W. D. (1971) Catalytic conversion of fatty acids to petroleum-like paraffins and their maturation. *Nat. Phys. Sci.* **232**, 140–144.

Shipp J., Gould I. R., Herckes P., Shock E. L., Williams L. B. and Hartnett H. E. (2013) Organic functional group transformations in water at elevated temperature and pressure: Reversibility, reactivity, and mechanisms. *Geochim. Cosmochim. Acta* **104**, 194–209.

Shipp J. A., Gould I. R., Shock E. L., Williams L. B. and Hartnett H. E. (2014) Sphalerite is a geochemical catalyst for carbon-hydrogen bond activation. *Proc. Natl. Acad. Sci. USA* **111**, 11642–11645.

Shock E. L. (1988) Organic acid metastability in sedimentary basins. *Geology* **16**, 886–890.

Shock E. L. (1989) Corrections to "Organic acid metastability in sedimentary basins". *Geology* **17**, 572–573.

Shock E. L. (1994) Application of thermodynamic calculations to geochemical processes involving organic acids. In *Organic Acids in Geological Processes* (eds. E. D. Pittman and M. D. Lewan). Springer-Verlag, Berlin, pp. 270–318.

Shock E. L. (1995) Organic acids in hydrothermal solutions: Standard molal thermodynamic properties of carboxylic acids, and estimates of dissociation constants at high temperatures and pressures. *Am. J. Sci.* **295**, 496–580.

Shock E. L. and Boyd E. S. (2015) Principles of geobiochemistry. *Elements* **11**, 395–401.

Shock E. and Canovas P. (2010) The potential for abiotic organic synthesis and biosynthesis at seafloor hydrothermal systems. *Geofluids* **10**, 161–192.

Shock E. L. and Helgeson H. C. (1990) Calculation of the thermodynamic and transport properties of aqueous species at high pressures and temperatures: Standard partial molal properties of organic species. *Geochim. Cosmochim. Acta* **54**, 915–945.

Shock E. L., Canovas P., Yang Z., Boyer G., Johnson K., Robinson K., Fecteau K., Windman T. and Cox A. (2013) Thermodynamics of organic transformations in hydrothermal fluids. *Rev. Mineral. Geochem.* **76**, 311–350.

Simkus D. N., Slater G. F., Sherwood Lollar B., Wilkie K., Kieft T. L., Magnabosco C., Lau M. C. Y., Pullin M. J., Hendrickson S. B., Wommack K. E., Sakowski E. G., van Heerden E., Kuloyo O., Linage B., Borgonie G. and Onstott T. C. (2016) Variations in microbial carbon sources and cycling in the deep continental subsurface. *Geochim. Cosmochim. Acta* **173**, 264–283.

Siskin M. and Katritzky A. R. (1991) Reactivity of organic compounds in hot water: Geochemical and technological implications. *Science* **254**, 231–237.

Smith M. B. and March J. (2007) *March's Advanced Organic Chemistry: Reactions, Mechanisms, and Structure*. Wiley-Interscience, Hoboken, New Jersey.

Somerville H. J., Bennett D., Davenport J. N., Holt M. S., Lynes A., Mahieu A., McCourt B., Parker J. G., Stephenson R. R., Watkinson R. J. and Wilkinson T. G. (1987) Environmental effect of produced water from North Sea oil operations. *Mar. Pollut. Bull.* **18**, 549–558.

Souza F. L., Preiner M. and Martin W. F. (2018) Native metals, electron bifurcation, and CO_2 reduction in early biochemical evolution. *Curr. Opin. Microbiol.* **43**, 77–83.

Stermitz F. R. and Huang W. H. (1971) Thermal and photode-carboxylation of 2-, 3-, and 4-pyridylacetic acid. *J. Am. Chem. Soc.* **93**, 3427–3431.

Straub T. S. and Bender M. L. (1972) Cycloamyloses as enzyme models. The decarboxylation of phenylcyanoacetate anions. *J. Am. Chem. Soc.* **94**, 8875–8881.

Streitwieser, Jr., A. and Koch H. F. (1964) Acidity of hydrocarbons. X. Exchange rates of ring-substituted toluene-α-t's with lithium cyclohexylamide in cyclohexylamine. *J. Am. Chem. Soc.* **86**, 404–409.

Streitwieser A. and Ni J. X. (1985) Base-catalyzed hydrogen isotope exchange and the aqueous acidity of toluene. *Tetrahedron Lett.* **26**, 6317–6320.

Strømgren T., Sørstrøm S. E., Schou L., Kaarstad I., Aunaas T., Brakstad O. G. and Johansen Ø. (1995) Acute toxic effects of produced water in relation to chemical composition and dispersion. *Mar. Environ. Res.* **40**, 147–169.

Suzuki Y., Konno U., Fukuda A., Komatsu D. D., Hirota A., Watanabe K., Togo Y., Morikawa N., Hagiwara H., Aosai D., Iwatsuki T., Tsunogai U., Nagao S., Ito K. and Mizuno T. (2014) Biogeochemical signals from deep microbial life in terrestrial crust. *PLoS ONE* **9**, e113063. https://doi.org/10.1371/journal.pone.0113063.

Sverjensky D. A., Stagno V. and Huang F. (2014) Important role for organic carbon in subduction-zone fluids in the deep carbon cycle. *Nat. Geosci.* **7**, 909–913.

Taylor P. J. (1972a) The decarboxylation of some heterocyclic acetic acids. *J. Chem. Soc. Perk. Trans. II* **9**, 1077–1086.

Taylor R. (1972b) Kinetics of electrophilic aromatic substitution. In *Comprehensive Chemical Kinetics: Reactions of Aromatic Compounds* (eds. C. H. Bamford and C. F. H. Tipper). Elsevier Publishing Company, Amsterdam, pp. 1–406.

Thibblin A. and Jencks W. P. (1979) Unstable carbanions. General acid catalysis of the cleavage of 1-phenylcyclopropanol and 1-phenyl-2-arylcyclopropanol anions. *J. Am. Chem. Soc.* **101**, 4963–4973.

Thorn K. A. and Aiken G. R. (1998) Biodegradation of crude oil into nonvolatile organic acids in a contaminated aquifer near Bemidji, Minnesota. *Org. Geochem.* **29**, 909–931.

Tissot B. P. and Welte D. H. (1984) *Petroleum Formation and Occurrence*. Springer-Verlag, Berlin.

Trembath-Reichert E., Morono Y., Ijira A., Hoshino T., Dawson K. S., Inagaki F. and Orphan V. J. (2017) Methyl-compound use and slow growth characterize microbial life in 2-km-deep subseafloor coal and shale beds. *Proc. Nat. Acad. Sci. USA* **114**, E9206–E9215.

Tully B. J., Wheat C. G., Glazer B. T. and Huber J. A. (2018) A dynamic microbial community with high functional redundancy inhabits the cold, oxic seafloor aquifer. *ISME J.* **12**, 1–16.

Ulrich G. and Bower S. (2008) Active methanogenesis and acetate utilization in Powder River Basin coals, United States. *Int. J. Coal Geol.* **76**, 25–33.

Utvik T. I. R. (1999) Chemical characterization of produced water from four offshore oil production platforms in the North Sea. *Chemosphere* **39**, 2593–2606.

Varsányi I., Kovács L. Ó., Kárpáti Z. and Matray J.-M. (2002) Carbon forms in formation waters from the Pannonian Basin, Hungary. *Chem. Geol.* **189**, 165–182.

Venturi S., Tassi F., Gould I. R., Shock E. L., Hartnett H. E., Lorance E. D., Bockisch C., Fecteau K. M., Capecchiacci F. and Vaselli O. (2017) Mineral-assisted production of benzene under hydrothermal conditions: Insights from experimental studies on C_6 cyclic hydrocarbons. *J. Volcanol. Geoth. Res.* **346**, 21–27.

Vieth A., Mangelsdorf K., Sykes R. and Horsfield B. (2008) Water extraction of coals – potential for estimating low molecular weight organic acids as carbon feedstock for the deep terrestrial biosphere. *Org. Geochem.* **39**, 985–991.

Walsh E. A., Kirkpatrick J. B., Pockalny R., Sauvage J., Spivack A. J., Murray R. W., Sogin M. L. and D'Hondt S. (2016) Relationship of bacterial richness to organic degradation rate and sediment age in subseafloor sediment. *Appl. Environ. Microbiol.* **82**, 4994–4999.

Walter S. R. S., Jaekel U., Osterholz H., Fisher A. T., Huber J. A., Pearson A., Dittmar T. and Girguis P. R. (2018) Microbial decomposition of marine dissolved organic matter in cool organic crust. *Nat. Geosci.* **11**, 334–339.

Watanabe M., Iida T. and Inomata H. (2006) Decomposition of a long chain saturated fatty acid with some additives in hot compressed water. *Energ. Convers. Manage.* **47**, 3344–3350.

Weiss M. C., Sousa F. L., Mrnjavac N., Neukirchen S., Roettger M., Nelson-Sathi S. and Martin W. F. (2016) The physiology and habitat of the last universal common ancestor. *Nat. Microbiol.* **1**, 16116. https://doi.org/10.1038/nmicrobiol.2016.116.

Wellsbury P., Goodman K., Barth T., Cragg B. A., Barnes S. P. and Parkes R. J. (1997) Deep marine biosphere fueled by increasing organic matter availability during burial and heating. *Nature* **388**, 573–576.

Willey L. M., Kharaka Y. K., Presser T. S., Rapp J. B. and Barnes I. (1975) Short chain aliphatic acid anions in oil field waters and their contribution to the measured alkalinity. *Geochim. Cosmochim. Acta* **39**, 1707–1711.

Willi A. V. (1959) Kinetics and mechanism of the decarboxylation of salicylic acids. *Trans. Faraday Soc.* **55**, 433–441.

Willi A. V. (1977) Homogeneous catalysis of organic reactions (mainly acid-base). In *Comprehensive Chemical Kinetics: Proton Transfer* (eds. C. H. Bamford and C. F. H. Tipper). Elsevier Scientific Publishing Company, Amsterdam, pp. 1–95.

Williams L. B., Hervig R. L., Holloway J. R. and Hutcheon I. (2001) Boron isotope geochemistry during diagenesis. Part I. Experimental determination of fractionation during illitization of smectite. *Geochim. Cosmochim. Acta* **65**, 1769–1782.

Wolfenden R., Lewis C. A. and Yuan Y. (2011) Kinetic challenges facing oxalate, malonate, acetoacetate, and oxaloacetate decarboxylases. *J. Am. Chem. Soc.* **133**, 5683–5685.

Wouters K., Moors H., Boven P. and Leys N. (2013) Evidence and characteristics of a diverse and metabolically active microbial community in deep subsurface clay borehole water. *FEMS Microbiol. Ecol.* **86**, 458–473.

Yang Z., Gould I. R., Williams L. B., Hartnett H. E. and Shock E. L. (2012) The central role of ketones in reversible and irreversible hydrothermal organic functional group transformations. *Geochim. Cosmochim. Acta* **98**, 48–65.

Yang Z., Lorance E. D., Bockisch C., Williams L. B., Hartnett H. E., Shock E. L. and Gould I. R. (2014) Hydrothermal photochemistry as a mechanistic tool in organic geochemistry: The chemistry of dibenzyl ketone. *J. Org. Chem.* **79**, 7861–7871.

Yang Z., Hartnett H. E., Shock E. L. and Gould I. R. (2015) Organic oxidations using geomimicry. *J. Org. Chem.* **80**, 12159–12165.

Yang Z., Williams L. B., Hartnett H. E., Gould I. R. and Shock E. L. (2018) Effects of iron-containing minerals on hydrothermal reactions of ketones. *Geochim. Cosmochim. Acta* **223**, 107–126.

Yasaka Y., Yoshida K., Wakai C., Matubayasi N. and Nakahara M. (2006) Kinetic and equilibrium study on formic acid decomposition in relation to the water-gas-shift reaction. *J. Phys. Chem. A* **110**, 11082–11090.

Zeng Y. and Liu J. (2000) Short-chain carboxylates in fluid inclusions in minerals. *Appl. Geochem.* **15**, 13–25.

Zeng Y., Liu J. and Zhu Y. (2002) Short-chain carboxylates in high-temperature ore fluids of W-Sn deposits in south China. *Geochem. J.* **36**, 219–234.

Zhu Y., Vieth-Hillebrand A., Wilke F. D. H. and Horsfield B. (2015) Characterization of water-soluble organic compounds released from black shales and coals. *Int. J. Coal Geol.* **150–151**, 265–275.

Zinke L. A., Reese B. K., McManus J., Wheat C. G., Orcutt B. N. and Amend J. P. (2018) Sediment microbial communities influenced by cool hydrothermal fluid migration. *Front. Microbiol.* **9**, 1249. https://doi.org/10.3389/fmicb.2018.01249.

Associate editor: Jean-francois Boily